Available online at www.sciencedirect.com
SCIENCE DIRECT
Geochimica et Cosmochimica Acta 70 (2006) 3075–3095
Geochimica
www.elsevier.com/locate/gca

Metamorphic fluid flow in the northeastern part of the 3.8–3.7 Ga Isua Greenstone Belt (SW Greenland): A re-evalution of fluid inclusion evidence for early Archean seafloor-hydrothermal systems

Wouter Heijlen [a,*], Peter W.U. Appel [a], Maria-Luce Frezzotti [b], Andy Horsewell [c], Jacques L.R. Touret [d]

[a] *Geological Survey of Denmark and Greenland (GEUS), Øster Voldgade 10, 1350 Copenhagen, Denmark*
[b] *Dipartimento di Scienze della Terra, Universita di Siena, Via Laterina 8, 53100 Siena, Italy*
[c] *Technical University of Denmark (DTU), Department of Manufacturing Engineering and Management, 2800 Kgs. Lyngby, Denmark*
[d] *Musée de Mineralogy, Ecole des Mines, 60 Blvd. Saint Michel, F-75006 Paris, France*

Received 13 January 2006; accepted in revised form 7 April 2006

Abstract

Fluid inclusions in quartz globules and quartz veins of a 3.8–3.7 Ga old, well-preserved pillow lava breccia in the northeastern Isua Greenstone Belt (IGB) were studied using microthermometry, Raman spectrometry and SEM Cathodoluminescence Imaging. Petrographic study of the different quartz segregations showed that they were affected by variable recrystallization which controlled their fluid inclusion content. The oldest unaltered fluid inclusions found are present in vein crystals that survived dynamic and static recrystallization. These crystals contain a cogenetic, immiscible assemblage of CO_2-rich (+H_2O, +graphite) and brine-rich (+CO_2, +halite, +carbonate) inclusions. The gas-rich inclusions have molar volumes between 44.8 and 47.5 cm^3/mol, while the brine inclusions have a salinity of ~33 eq. wt% NaCl. Modeling equilibrium immiscibility using volumetric and compositional properties of the endmember fluids indicates that fluid unmixing occurred at or near peak-metamorphic conditions of ~460 °C and ~4 kbar. Carbonate and graphite were precipitated cogenetically from the physically separated endmember fluids and were trapped in fluid inclusions.

In most quartz crystals, however, recrystallization obliterated such early fluid inclusion assemblages and left graphite and carbonate as solid inclusions in recrystallized grains. Intragranular fluid inclusion trails in the recrystallized grains of breccia cementing and crosscutting quartz veins have CO_2-rich assemblages, with distinctly different molar volumes (either between 43.7 and 47.5 cm^3/mol or between 53.5 and 74.1 cm^3/mol), and immiscible, halite-saturated H_2O–CO_2–NaCl(–other salt) inclusions. Later intergranular trails have CH_4–H_2 (X_{H_2} up to ~0.3) inclusions of variable density (ranging from 48.0 to >105.3 cm^3/mol) and metastable H_2O–NaCl(–other salt?) brines (~28 eq. wt% NaCl). Finally, the youngest fluid inclusion assemblages are found in non-luminescent secondary quartz and contain low-density CH_4 (molar volume > 105.33 cm^3/mol) and low-salinity H_2O–NaCl (0.2–3.7 eq. wt% NaCl). These successive fluid inclusion assemblages record a retrograde *P–T* evolution close to a geothermal gradient of ~30 °C/km, but also indicate fluid pressure variations and the introduction of highly reducing fluids at ~200–300 °C and 0.5–2 kbar. The quartz globules in the pillow fragments only contain sporadic CH_4(+H_2) and brine inclusions, corresponding with the late generations present in the cementing and crosscutting veins. We argue that due to the large extent of static recrystallization in quartz globules in the pillow breccia fragments, only these relatively late fluid inclusions have been preserved, and that they do not represent remnants of an early, seafloor-hydrothermal system as was previously proposed.

Modeling the oxidation state of the fluids indicates a rock buffered system at peak-metamorphic conditions, but suggests a change towards fluid–graphite disequilibrium and a $\log f_{H_2}/f_{H_2O}$ above the Quartz–Fayalite–Magnetite buffer during retrograde evolution. Most likely, this indicates a control on redox conditions and on fluid speciation by ultramafic rocks in the IGB.

* Corresponding author. Present address: School of Earth and Environment, University of Leeds, Woodhouse Lane, Leeds LS2 9JT, United Kingdom.
E-mail address: W.Heijlen@earth.leeds.ac.uk (W. Heijlen).

0016-7037/$ - see front matter
doi:10.1016/j.gca.2006.04.005

Finally, this study shows that microscopic solid graphite in recrystallized metamorphic rocks from Isua can be deposited inorganically from a fluid phase, adding to the complexity of processes that formed reduced carbon in the oldest, well-preserved supracrustal rocks on Earth.

1. Introduction

Early Archean rocks can provide clues to processes operating in the early evolution of our planet and to environmental conditions that sustained development of life. In search for the latter, the 3.8–3.7 Ga supracrustal rocks of the Isua Greenstone Belt (IGB) in South-West Greenland have played a highly debated role for the past 25 years (e.g. Moorbath, 2005). The light carbon isotopic composition of microscopic graphite in Isua rocks has been proposed as a biomarker (Schidlowski et al., 1979; Mojzsis et al., 1996; Rosing, 1999; Schidlowski, 2001; Ueno et al., 2002), but this has been seriously questioned and disproved in many cases (Perry and Ahmad, 1977; Lepland et al., 2002; Van Zuilen et al., 2002, 2003). Concerning the composition and evolution of the hydrosphere, analyses of fluid inclusions in minerals from the ~3.5 Ga North Pole Dome (Foriel et al., 2004) and the ~3.2 Ga Barberton Greenstone Belt (Channer et al., 1997; De Ronde et al., 1997) have been interpreted as evidence that the composition of seawater varied considerably during the Archean. Fluid inclusions analyzed in these studies were present in undeformed and virtually unmetamorphosed quartz-filled vugs in pillow lavas and ironstone pods, respectively. However, greenstone belts older then ~3.5 Ga have all been subjected to high or intermediate grade metamorphism, complicating the interpretation of fluid inclusion data.

Appel et al. (1998, 2001) and Touret (2003) described a well-preserved occurrence of pillow lavas and pillow lava breccia in a low-strain zone in the northeastern IGB, and provided first results of a fluid inclusion study on quartz ''vesicles'' in pillow fragments. In this paper, the non-genetic term ''globules'' is preferred to ''vesicles'', though the globules studied here correspond with the ''vesicles'' described by Appel et al. (2001) and Touret (2003). Although these quartz globules were clearly affected by extensive recrystallization, the previous studies reported that they contained an immiscible assemblage of methane and brines. This was somewhat surprising given the mineralogy and metamorphic grade of the host-rocks (lower amphibolite facies). The breccia cementing quartz veins, in contrast, were reported to have mainly CO_2-rich inclusions, which were interpreted as peak-metamorphic fluids. Since methane-dominated fluids are unlikely to be stable at peak-metamorphic conditions of the lower amphibolite facies, Appel et al. (2001) and Touret (2003) suggested that the fluid inclusions contained in the pillow globules could have remnants of early, seafloor-hydrothermal brines and gasses, that, although being re-equilibrated with respect to density, essentially survived quartz recrystallization.

In this study, we focus on the relation between the microstructural evolution of the quartz globules and veins and the preservation of contained fluid inclusions. Furthermore, we attempt to constrain the metamorphic fluid flow at the pillow breccia locality more completely. The results of this study question the previous interpretation and suggest that the oldest fluid inclusions at this locality were trapped at peak-metamorphic conditions. We propose that the difference between typologic groups and amounts of fluid inclusions present in quartz globules and cementing veins is strongly controlled by the extent of quartz recovery. Moreover, the new interpretation of the fluid flow paragenesis enables reconstruction of the retrograde metamorphic P–T evolution of the breccia occurrence, and offers some compelling evidence for fluid-deposited microscopic graphite and carbonate at this locality.

2. Regional geology

The IGB is the largest of the numerous >3.6 Ga supracrustal enclaves in the Itsaq Gneiss Complex of in southern West Greenland (Nutman et al., 2002; Friend and Nutman, 2005). This complex represents a large suite of tonalite–trondhjemite–granodiorite gneisses with emplacement ages between 3.85 and 3.56 Ga (Friend et al., 1996; Nutman et al., 1996, 2002). They show both intrusive and tectonic contacts with the supracrustal rocks at Isua. Protoliths of the IGB include basaltic and high Mg-basaltic pillow lava and pillow lava breccia, cherts, banded-iron formation (BIF), ultramafic rocks, and minor sedimentary strata, such as conglomerates and garnet–mica–schists (Myers, 2002). The rocks are mostly strongly deformed and have been metamorphosed up to amphibolite facies, but despite this they have been reliably dated between 3.7 and 3.8 Ga (Moorbath et al., 1973, 1977; Nutman et al., 1996, 2002). Several episodes of metasomatism affected the supracrustal rocks, some of which could have been related to seafloor-hydrothermal events (Appel et al., 2001), others to metamorphic/magmatic fluid flow contemporaneous with tonalite emplacement (e.g. Frei et al., 2002) or spatially associated with ultramafic rocks (Rose et al., 1996; Rosing et al., 1996). Peak-metamorphic P–T conditions for various parts of the IGB range from 380 to 600 °C at pressures between ~3.5 and 7 kbar (Boak and Dymek, 1982; Gruau et al., 1996; Hayashi et al., 2000; Appel et al., 2001; Rollinson, 2002, 2003). Rollinson (2002, 2003) made a systematic study of garnet zoning in the IGB and distinguished 5 tectono-metamorphic domains separated by ductile faults.

Of special importance is his Domain 1, located in the northeastern part of the belt (Fig. 1), because it has the lowest

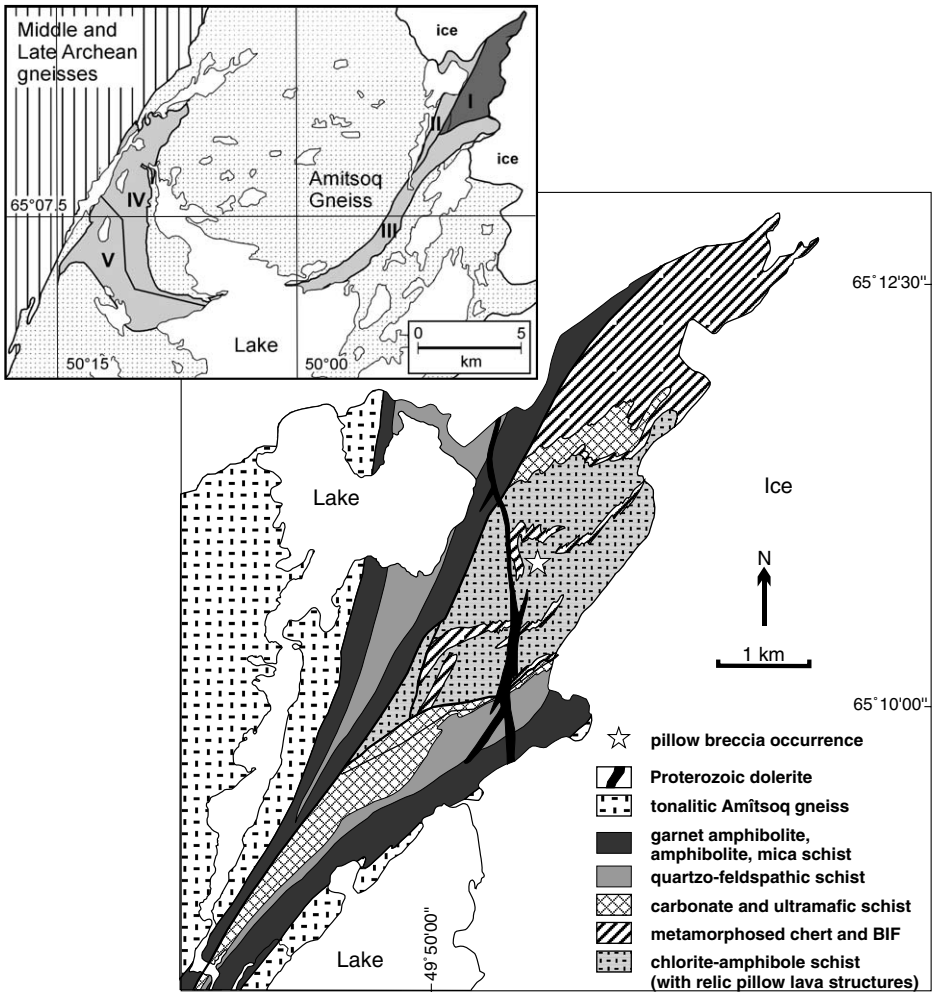

Fig. 1. Geologic map from the low-strain zone (I in inset) in the eastern part of the IGB (Solvang, 1999). Location of the investigated pillow breccia occurrence is indicated by a star. Inset shows a simplified overview of the IGB (grey areas), with indication of the five areas that have a distinct metamorphic history (Rollinson, 2003).

degree of metamorphism and is characterized by only one Early Archean metamorphic event. This domain has also been least deformed (Nutman et al., 2002) and contains the low-strain zone in which volcano-sedimentary structures (i.e. pillow breccia occurrence, Fig. 2) are well preserved (Appel et al., 1998). For the pillow breccia outcrop, Appel et al. (2001) calculated peak-metamorphic temperatures and pressures ranging between 430 and 500 °C, at 3.6 to 4.4 kbar, based on mineral composition and garnet–biotite geothermometry. The timing of the Early Archean metamorphism is not known precisely, but most likely is between ~3.63 and 3.62 Ga (Crowley, 2003). Deformed rocks in the northeastern IGB are cut by doleritic dykes (Ameralik dyke swarm). These dykes probably were emplaced during several periods in the Mesoarchean, but in the Isua area were most likely formed at ~3.51 Ga (Nutman et al., 2004).

Fig. 2. Photograph of the pillow breccia and its cementing quartz. Note the amygloidal structure of the pillow fragments, the sharp outline and the dark rim in one of the fragments. Length of the photograph is ~0.5 m.

3. Analytical techniques

For fluid inclusion studies, 40 doubly polished wafers were studied from a weakly deformed pillow breccia specimen and from cementing and crosscutting quartz veins. Microthermometric measurements were made on a Linkam THMSG 600 heating-freezing stage mounted on a Leitz Orthoplan microscope at the University of Copenhagen (Denmark). Following phase changes were measured: homogenization of the carbonic

phases Th_{CO_2} or Th_{CH_4}) into the liquid phase (e.g. $liqCO_2 + vapCO_2 = liqCO_2$), into the vapor phase (e.g. $liqCO_2 + vapCO_2 = vapCO_2$), or by critical homogenization (e.g. $liqCO_2 + vapCO_2 =$ supercritical CO_2), final melting of the carbonic phase (Tm_{CO_2}), first melting of the aqueous solution (T_{fm}), final melting of ice (Tm_{ice}), final melting of clathrates (Tm_{clath}), final melting of hydrohalite (Tm_{hh}), dissolution of halite (Ts_{halite}) and, in a few cases, total homogenization of the aqueous and carbonic fluid phases (Th_{tot}; simply abbreviated as Th if no carbonic phase was present). The stage was calibrated with synthetic CO_2–H_2O (Tm_{CO_2}) and Na–Ca–Cl brine fluid inclusions (Tm_{ice}). In addition, the melting point of an indium standard was used as a calibration point (Tm: 156 °C). Heating rates during microthermometric runs were between 0.1 and 0.5°/min. Cryogenic measurements were always done first, before SEM-CL or Raman study. As it was suspected that many gas inclusions had an aqueous phase, not optically visible, Th_{CO_2} measurements were made after cooling the inclusions only to ~−25 °C (in metastable absence of clathrates, e.g. Diamond, 2003a). Th and/or Ts measurements on brine inclusions were made after all other studies. For determination of (Tm_{clath}) a cycling technique was used. Most measurements on gaseous inclusions and all measurements on aqueous inclusions were checked for reproducibility. Volume percentages were extrapolated from 2-dimensional photographs using image analysis. Calculation of compositional/volumetric properties and isochores were made using the software package FLUIDS, developed by R. Bakker (Bakker, 2003; Bakker and Brown, 2003).

Wafers and additional thin sections were investigated by SEM-Cathodoluminescence (SEM-CL) at the Technical University of Denmark (DTU, Kgs. Lyngby, Denmark), using a JEOL JSM-5900 SEM equipped with a GATAN mini Cathodoluminescence detector. In general, the working distance was 24 mm and acceleration voltage 20 kV.

Selected fluid and solid inclusions were analyzed by Raman spectrometry at the University of Siena (Siena, Italy) using a Confocal Labram Multichannel spectrometer (Jobin-Yvon LTD). An Ar^+ ion laser produced the excitation line at 514.5 nm (emission power: 2.5 W). Raman intensity was collected by a Peltier-cooled CCD detector. The scattered light was analyzed using a Notch holographic filter with a spectral resolution of 1.5 cm^{-1} and grating of 1800 groves/mm. The laser was focused by an Olympus 100x lens to a spot size of ~1–2 μm.

C–O–H speciations and fugacity calculations were made using SUPCRT92 (Johnson et al., 1992), with upgraded database, and using fugacity coefficients by Ryzhenko and Volkov (1971) and Shi and Saxena (1992).

4. Microstructure of quartz seggregations in the pillow breccia

The field occurrence of the weakly deformed pillow breccia has been described by Appel et al. (1998, 2001) and a detailed petrographic description of the rocks and their different quartz segregations was given by Appel et al. (2001) and Touret (2003). Fig. 2 shows a picture of the outcrop, which is located in the "low-strain zone" described by Appel et al. (1998). The largest exposure of the pillow breccia is ~10 m^2. The breccia grades into pillows with interstitial quartz-bearing material. It has a stretching lineation defined by elongated quartz globules and pillow fragments, which plunges southeast. The breccia is clast-supported and the clasts are medium-grained pillow fragments with sharp and well-defined edges. These fragments are cemented by white, granular quartz with some minor carbonate (termed here cementing quartz veins). Some cm to tens of cm wide, coarser grained quartz veins are crosscutting the breccia in various directions (crosscutting quartz veins). Below, we give a brief summary of the microtexture of the different varieties of veins and globules, previously described by Appel et al. (2001) and Touret (2003), but incorporate additional SEM-CL observations, and emphasize the difference in recrystallization of quartz grains in cementing and crosscutting veins, and in the globules.

4.1. Cementing and crosscutting quartz veins

The cementing quartz veins are made up of more or less equidimensional grains which show mostly straight extinction under crossed polars. Sometimes, however, they are more strained, have undulous extinction and some subgrains. They have irregular to straight grain boundaries and are loaded with 10–50 μm large solid carbonate inclusions. Fluid inclusions are rare in these crystals and if present, are mostly located along intragranular and intergranular trails.

Quartz in the crosscutting veins has a bimodal grain size distribution, with a few large grains surrounded by lots of smaller equigranular crystals (Fig. 3A). In thin section, the larger grains have a dirty appearance, due to many planar and clustered Fluid Inclusion Assemblages (FIA's). Internally, they have undulous extinction or consist of many subgrains (Fig. 3C). They also have irregular, lobate grain boundaries, which are decorated with rounded to irregular, dark gaseous and small aqueous inclusions. In contrast, smaller grains are clear, have straight extinction and approach a granoblastic polygonal texture with smoothly curved boundaries, which frequently meet in triple junctions at 120°. They have a much smaller amount of fluid inclusions. Small grains may bulge into adjacent larger grains, and sometimes unstrained, clear crystals have nucleated and grown into the strained larger crystals, obliterating subgrain boundaries and fluid inclusion trails. However, the unstrained, granoblastic grains have numerous, 10–50 μm large solid inclusions, mainly carbonates, that are typically absent in the larger, strained crystals. In general, smaller grains in these veins are similar to the ones in the cementing veins. Both large, strained grains and small, unstrained grains show an inhomogeneous, dull luminescent pattern (Fig. 3D). The luminescent character is, nevertheless, specific for each grain. Note that most highly luminescent spots in Fig. 3D, are artifacts corresponding to open fractures or holes in the sample surface. In general, large strained grains show a mottling pattern, while smaller, unstrained crystals have a very dull core and more moderate luminescent rim, both in the cementing and croscutting veins. In all varieties of quartz from the different types of veins, a network of non-luminescent, healed microfractures can be seen (Fig. 3D). These healed fractures are mainly located near grain boundaries but also crosscut strained and unstrained grains.

The petrographic observations indicate that the fine-grained, clear quartz have arisen from extensive dynamic and secondary static recrystallization of the vein quartz

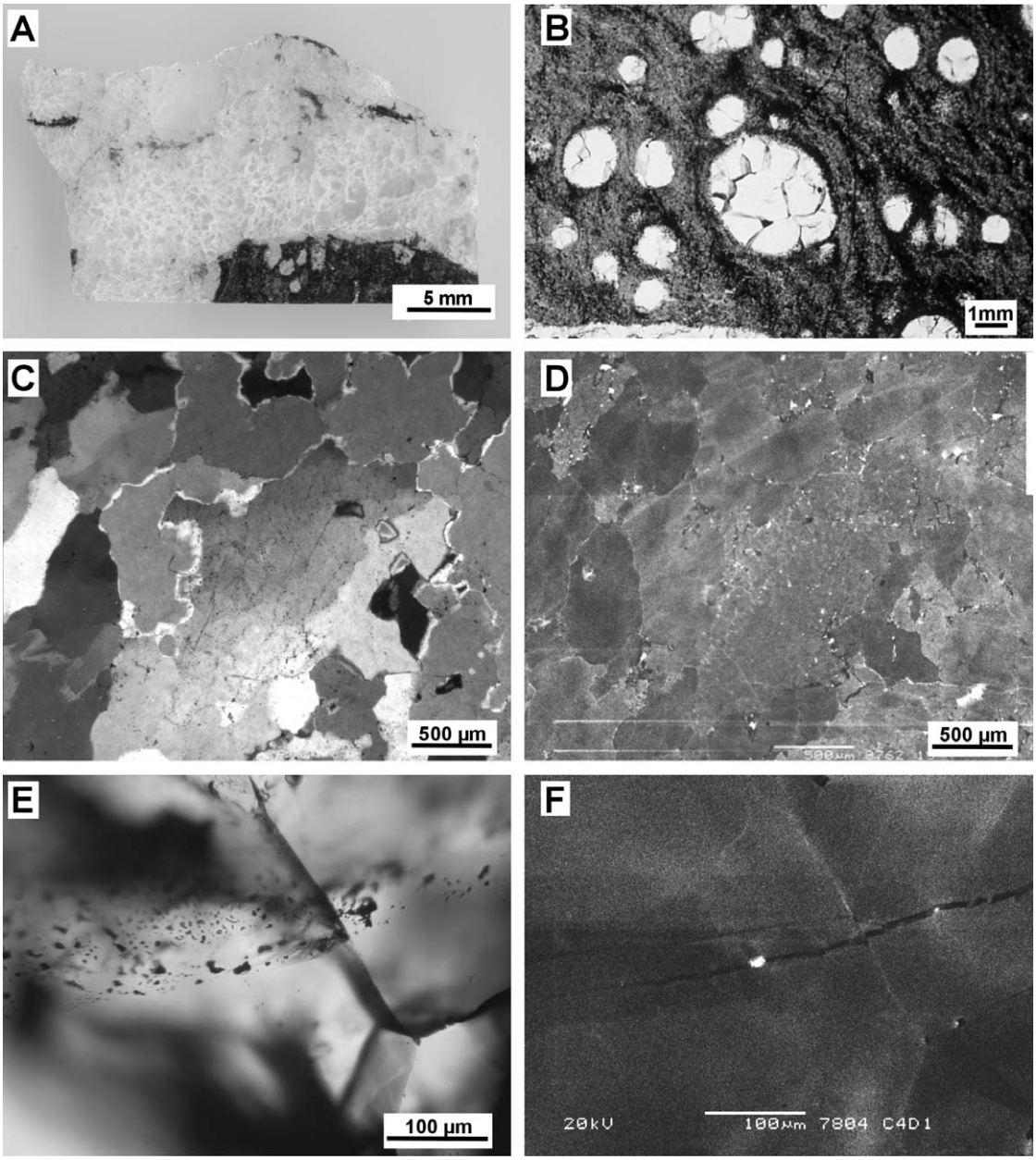

Fig. 3. (A) Thick section (300 µm) of a thin cementing and crosscutting quartz vein, and a pillow fragment. The crosscutting vein quartz is located at the top of the section and has a bimodal grain size distribution. The smaller sized crystal of the cementing veins are surrounding the pillow fragment. (B) Occurrence of mono- and multicrystalline quartz globules in the pillow fragments. Equidimensional quartz grains have smooth grain boundaries and show a foam network, indicating static recovery. (C) Thin section microphotographs (crossed polars) of a large, strained crystal in the crosscutting quartz veins and surrounding, recrystallized grains. Note the abundance of fluid inclusion trails and clusters in the large grain compared to the recrystallized ones. (D) SEM-CL image of C, showing the more or less homogeneous, dull-luminescent character of the recrystallized grains, the mottled appearance of the strained grain and the non-luminescent secondary quartz in healed fractures. Note that highly luminescent spots are due to holes in the sample surface. (E) Transmitted light photograph of quartz grains and triple junction in the quartz globules, having a late, intergranular trail of G_2^V–W_3 inclusions. (F) SEM-CL image of E showing the non-luminescent expression of the healed microfracture.

(Drury and Urai, 1990; Passchier and Trouw, 1996), a process which seems to have proceeded to a higher degree in the cementing veins. In the later crosscutting veins, large grains are deformed and fragmented by subgrain rotation recrystallization and by grain boundary migration, but essentially survived complete recrystallization. Overall, dynamic recrystallization phenomena found in vein quartz correspond to Regime 3 of Hirth and Tullis (1992). The tendency for straightening of grain boundaries (sometimes with a curvature) and occurrence of well-formed triple junctions, indicates that secondary static recrystallization also played a role. The healed fractures of non-luminescent, secondary quartz are clearly representative of the latest event that affected the vein crystals.

4.2. Quartz globules in pillow fragments

The pillow fragments are made up of a biotite–muscovite–quartz matrix containing minor garnet, ilmenite, calcite, chalcopyrite and pyrrhotite. They have abundant, variably sized quartz globules, 1–10 mm in longest direction (Fig. 3B). The globules can be perfectly spherical, but more commonly are ellipsoidal or have an irregular shape. Some have an angular outline, indicating pseudomorphic replacement of former phenocrysts (Appel et al., 2001). When globules are elliptical in thin section, they are flattened parallel to a faint schistosity.

Small (~1 mm) globules comprise one or two big quartz grains, yet larger, granoblastic globules can have some tens of crystals that form an equigranular to inequigranular polygonal (foam) structure. Sometimes large (50–500 μm) biotite, muscovite, calcite, tourmaline, chalcopyrite or pyrrhotite crystals (the latter often rimmed by Fe-oxides) or aggregates can be found in the centre, or near the rim of the globules. The quartz is often very clear, rendering it black in hand specimen (e.g. Appel et al., 2001). Nevertheless, it frequently contains small rounded, elliptical, polygonal and prismatic solid inclusions, typically ~10 to 50 μm in long dimension. Most of these are carbonates, similar to those in the quartz veins. Biphase aqueous inclusions containing one or more highly birefringent solids can sometimes be found within a cluster of solid inclusions, but in comparison with the quartz veins, fluid inclusions are exceedingly rare in the globule quartz.

Using cathodoluminescence imaging, the quartz grains generally show weak undulous luminescence, specific for each grain. Sometimes, higher luminescent patches can be seen. Touret (2003) reported preliminary CL-observations of globules that had an apparent geodic lining of the quartz grains. Both monocrystalline and multicrystalline globules were reported to have distinct luminescent bands parallel to the globule wall. Similar arrangements of quartz crystals in the globules were observed, but no such luminescent bands were found in this study, although different working conditions of the SEM were attempted. Furthermore, no CL microstructures were found in relation to intragranular fluid inclusion trails, clusters or isolated fluid inclusions. Only late, healed fractures are visible as they are made up of secondary, non-luminescent quartz and show a sharp contrast with the dull luminescent matrix. As can be seen in Figs. 3E and F, such healed quartz fractures can be followed through different grains, but show a small displacement at grain boundaries. Mostly, they have a distinct orientation at high angle to the direction of flattening of the host globule.

The petrographic study indicates that, in contrast to the cementing, and especially the crosscutting veins, quartz grains in the pillow globules show nearly complete recovery and annulation of possible earlier deformation microstructures. Based on the relatively large grain size of most crystals, the smooth and slightly curved grain boundaries, the equilibrated triple junctions, the resemblance to a foam structure of multicrystalline globules, and the fact that unstrained crystals occur in all globules regardless of their form (spherical, elliptical, angular and irregular), grain boundary area reduction (GBAR)—principal mechanism of static recrystallization (Passchier and Trouw, 1996)—seems to have been the dominant recovery mechanism. Recrystallization seems to have obliterated all pre-existing intra- and intercrystalline structures.

5. Fluid inclusion study

5.1. Fluid inclusion typology

Gaseous and aqueous fluid inclusions were found in both the cementing and crosscutting quartz veins, and in pillow fragment globules. Although some modifications exist, the inclusions found can be subdivided in five typologic types.

5.1.1. G_1 inclusions

Inclusions of this type consist dominantly of CO_2, sometimes with up to a few mol% CH_4. They are mono- or biphase at room temperature and have often a perfect negative crystal shape. In general, they are 5–30 μm large. All inclusions found in this study homogenized to the

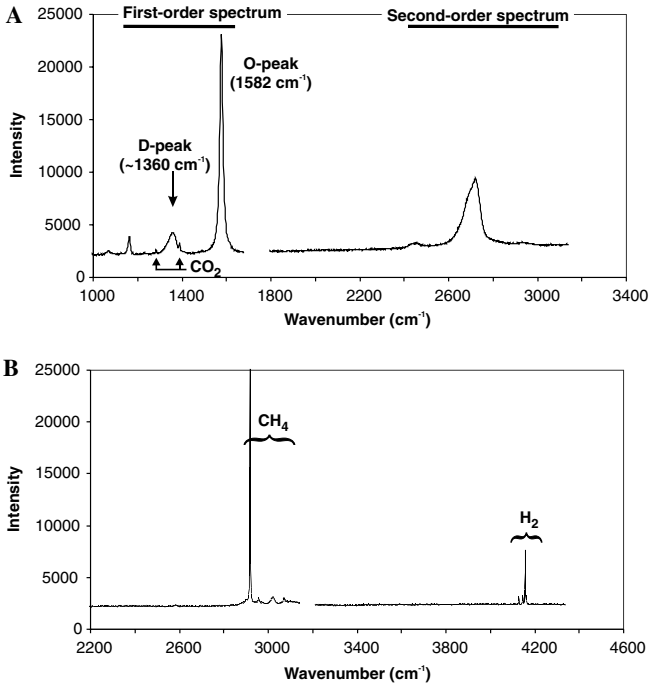

Fig. 4. (A) Representative first- and second-order Raman spectrum of graphite in a G_1 inclusion. A small expression of the fermi-diad of the CO_2 phase is still present. O-peak refers to ordered peak, while D-peak indicates the disordered peak (e.g. Pasteris and Chou, 1998). (B) Raman spectrum of a G_2 inclusion, showing clear fundamental vibrations of CH_4 (2917 cm^{-1}) and H_2 (4156 cm^{-1}).

liquid. Furthermore, they sometimes have an optically visible aqueous phase wetting the inclusion walls. In strained, remnant crystals of the quartz veins, they frequently have opaque, rounded solids that coalescence together to form framboidal aggregates occupying very variable volume percentages. Raman analyses showed that this solid is graphite (Fig. 4A) with a relatively high crystallinity (e.g. Luque et al., 1998; Pasteris and Chou, 1998; Pasteris, 1999).

5.1.2. G_2 inclusions

These gaseous inclusions contain CH_4. Furthermore, Raman analyses showed that most G_2 inclusions have no detectable CO_2, but a significant X_{H_2} (Fig. 4B), ranging between 0.03 and 0.28. As for G_1 inclusions, the G_2 inclusions often have a ne+gative crystal shape and appear quite large. Inclusions were found that homogenized to liquid (G_2^L), showed critical homogenization (G_2^C) or homogenized to vapor (G_2^V). Critical homogenization and homogenization to liquid could sometimes take place at temperatures significantly higher then the critical temperature of pure CH_4 (−82.6 °C). The maximum Th_{crit} recorded in this study was −78.3 °C.

5.1.3. W_1 inclusions

W_1 inclusions are water-dominated, and at room temperature have a gas phase of ~10 to 30 vol% and typically a cubic halite crystal (~10 vol%). Furthermore, they often contain one or more highly birefringent solids that can occupy a variable vol% of the inclusion. SEM-EDX and Raman analyses showed that these solids are carbonates, with varying Ca, Fe and Mg content. By far most W_1 inclusions found have CO_2 in the gas phase. Frequently, both liquid and vapor CO_2 are present at room temperature. However, in some inclusions only CH_4 could be detected. The inclusions often have a negative crystal shape, though this is not as common as for the gaseous inclusions. Their size varies greatly between <1 μm to 50 μm. Th_{tot} of W_1 inclusions could not be determined because they decrepitate on heating between ~220 and 300 °C. Also, this made measurement of Ts_{halite} difficult in many cases, while carbonates never dissolved up to the temperature of decrepitation. Ts_{halite} of few W_1 inclusions that did not decrepitate on heating was between 239 and 248 °C ($n = 4$), corresponding with a salinity of ~33 eq. wt% NaCl (Sterner et al., 1988).

During cooling, the liquid phase froze at ~−60 °C. The inclusions then had a speckled dark brown appearance and metastable halite. Reheating the inclusions caused the formation of a liquid at temperatures between −40 and −35 °C (T_{fm}). During further heating, the halite crystal first became rimmed by hydrohalite and eventually reacted completely in the temperature interval between −35 and −25 °C. Renewed cooling and heating of the stable assemblage (ice, hydrate(s), gas) indicated T_{fm} in the same range as when halite was present. Ice melted consistently around −24.5 °C. Tm_{clath} was between −15.5 and −6.1 °C ($n = 14$). Hydrohalite always persisted metastably to temperatures >0.1 °C (upper limit of hydrohalite stability), until it suddenly disappeared with the reappearance of one or more halite cubes.

5.1.4. W_2 inclusions

This type of aqueous inclusions have bubbles occupying 3–10 vol% at room temperature and only sporadic halite or some small, rounded bireflecting solids. The latter solids do not dissolve upon heating. Sometimes, a halite crystal appeared after cryogenic runs (see further). No CO_2 or CH_4 could be detected in the vapor phase, and no clathrates seemed to be present during cryogenic runs. Size and shape of the inclusions vary widely. Their melting behavior is distinctly different from W_1 inclusions and is characterized by metastability. Most W_2 inclusions did not freeze on heating to −180 °C, but sometimes inclusions crystallized after being kept at −80 °C for ~1 h. However, at any rate of heating or analytical protocol followed, first melting of a frozen inclusion always started around −75 to −70 °C. Ice melted at temperatures between −40.0 and −27.3 °C, but hydrohalite always remained present to temperatures >0.1 °C.

5.1.5. W_3 inclusions

W_3 inclusions are low-salinity aqueous inclusions. Frequently they are monophase, and sometimes, they have a small, moving gas bubble. These inclusions are typically associated with G_2^V inclusions, forming unmixable assemblages. Tm_{ice} for these inclusions ranged between −2.2 and −0.1 °C ($n = 11$).

5.2. Fluid inclusion occurrence and microthermometry

As commonly observed in metamorphic rocks, the distribution of typologic types of inclusions is complex, hence it should be described in relation to the microstructure of the host crystal (Touret, 1981, 2001; Marshall et al., 2000). We subdivide fluid inclusion assemblages in 2 groups, i.e. those assemblages fully contained within a single crystal (“intragranular”) and those that are distributed continuously between different grains (“intergranular”). Within a certain quartz segregation (e.g. a type of quartz vein or a quartz globule), intragranular FIA’s can be assumed to be older then intergranular FIA’s in the same crystals, since the latter were not completely transposed by quartz recrystallization. Furthermore, intergranular FIA’s can be subdivided in those that have no expression under SEM-CL and those that are associated with non-luminescent, secondary quartz. Again, the latter are younger since they were formed by healing of brittle microfractures in the end stage of ductile quartz recovery. The different FIA’s in the pillow breccia occurrence will be discussed as follows:

1. Intragranular FIA’s:
   - in remnant, strained crystals of the crosscutting quartz veins (oldest FIA’s in these veins);

- in recrystallized grains of the cementing and crosscutting quartz veins;
- in recrystallized grains in quartz globules (oldest FIA's in the globules).

2. Intergranular FIA's:
   - not visible using cathodoluminescence imaging;
   - visible (non-luminescent) using cathodoluminescence imaging.

Microthermometric measurements are summarized in Table 1.

5.2.1. Intragranular fluid inclusion assemblages

5.2.1.1. In strained crystals of the crosscutting quartz veins. Fluid inclusions are relatively abundant in the large, strained, remnant quartz crystals in crosscutting veins (e.g. Fig. 3C). Monophase G_1 FIA's are dominant. Frequently, they contain highly ordered graphite, which then occupies a variable volume percentage of the inclusion. Regardless of the presence or absence of a small aqueous phase or graphite, G_1 inclusions in strained crystals have indistinguishable volumetric and compositional properties of the gas phase. Tm_{CO2}-values are close to the CO_2 triple point. They ranged between −62.4 and −56.6 °C ($n = 41$) with a mode of −56.7 °C (Fig. 5A). Raman analyses showed that the depression in Tm_{CO2} is due to the presence of CH_4. Measured X_{CH_4} was up to 0.1 in these inclusions. Homogenization temperatures were between −22.0 and −2.2 °C ($n = 48$), but mostly vary between −2 and −10 °C (Fig. 5A). Furthermore, there seems to be a correlation between Tm_{CO2} and Th_{CO_2}. This suggests that the lowest Th_{CO_2} values are due to the (sporadic) higher CH_4 contents, and do not indicate lower molar volumes. Therefore, molar volumes of G_1 inclusions having $X_{CH_4} < 0.01$ range between 44.8 and 47.5 cm^3/mol.

Aside from assemblages having only G_1 inclusions, assemblages of mixed G_1 and W_1 inclusions are common (Figs. 5B–D and 6). In these assemblages, inclusions contain variable proportions of aqueous liquid + halite + carbonates + graphite + gas. It is striking that, if present, graphite is always located within the gas phase, while the aqueous phase has sometimes one or more variably sized carbonates (trapped crystals). Inclusions that are aqueous-dominated always have a halite crystal (~10 vol%), while halite is characteristically absent in CO_2-dominated inclusions (Fig. 5D). Tm_{clath} could only be measured on few CO_2-dominated inclusions and varied between −13.2 and 0.3 °C (Fig 5C; $n = 6$). The low Tm_{clath} could indicate that the liquid in some CO_2-dominated inclusions is metastable, halite saturated brine. If the empirical equation of Diamond (1992) can be extended to salinities >23.6 eq. wt% NaCl, combined Th_{CO_2} and Tm_{clath} indicate a salinity variation between 16.1 and ~30 eq. wt% NaCl, approaching the salinity typical for W_1 inclusions. Similar as for pure W_1 inclusions, aqueous-dominated W_1–G_1 inclusions decrepitated on heating (between 220 and 300 °C). As presented in Fig. 5D, fluid inclusions in G_1–W_1 assemblages show a negative correlation between vol% CO_2 and Th_{CO_2}, and this is independent of the presence or absence of graphite in the CO_2-phase. Because we suspect that most gas-dominated inclusions contain a small aqueous phase, we estimate the error in vol% CO_2 in Fig. 5D to be ~10% to 20%. Despite such an error, the negative trend demonstrates that the range in volumetric proportions of CO_2 in G_1–W_1 inclusions are not due to post-deformation stretching or leakage of H_2O (e.g. Bakker and Jansen, 1990, 1991; Hollister, 1990; Johnson and Hollister, 1995; Audétat and Günther, 1999), since such processes would result in a reverse trend. The combined decrease in density and vol% of the CO_2 phase (decrease of X_{CO_2}), together with an increase in salinity (halite present vs. not present) and the petrographic observation of coexistence of CO_2- and aqueous-dominated inclusions in the same FIA, provides strong evidence for equilibrium immiscibility (e.g. Pichavant et al., 1982; Ramboz et al., 1982; Huizenga and Touret, 1999). And the compositional/volumetric relationship must have been preserved during further retrograde evolution in the crystals that survived complete recovery. Tm_{CO2} of fluid inclusions in G_1–W_1 assemblages varied between −63.6 and −56.6 °C ($n = 41$). It is strongly clustered around −56.9 °C, and the lower values are due to the (sporadic) presence of CH_4.

5.2.1.2. In recrystallized grains of the cementing and crosscutting quartz veins. Compared to strained, remnant crystals, fluid inclusions are much less abundant in recrystallized, clear quartz grains. This is obvious in the cementing veins where fluid inclusions are mostly located along intragranular trails. In the crosscutting veins, it can be seen that fluid inclusion trails and clusters present in the strained crystals have been wiped out during the recovery process. Fig. 7 shows a detailed drawing of the distribution of intragranular trails and clusters in an unstrained, recrystallized grain. Most of the fluid (carbonic and aqueous) appears to have been remobilized and removed. Graphite, occurring within the fluid inclusions in strained crystals, is left behind as solid particles in three-dimensional clusters. Only few isolated or clustered aqueous- and carbonic-dominated inclusions remain, and these have very variable compositional and volumetric properties. Nearly always they contain a variably sized halite crystal and few carbonates. These inclusions often have a halo of tiny, sub-μm inclusions, yet frequently a regular negative crystal shape. They have probably undergone fluid leakage/and or stretching (e.g. Sterner et al., 1995; van den Kerkhof et al., 2004) and will not be discussed further. However, the recrystallized grains also contain straight to curved trails of W_1 and, more abundant, G_1 inclusions. Sometimes, few W_1 inclusions occur in a G_1 trail and vice versa, but no clear mixed inclusions were found. FIA's of G_1 inclusions show 2 distinct populations with different density of the CO_2 phase (Figs. 5G and 7). One population has Th_{CO_2} between −15 and 0 °C, while the other population has a much lower density (Th_{CO_2} between 15 and 30 °C).

Table 1
Microthermometric measurements (in °C) given as the range (min/max) and number of measurements (*n*)

Petrographic occurrence[a]	Type		Tm_{CO_2}	Tm_{clath}	Tm_{ice}	Th_{CO_2}[b]	Th_{CH_4}[b]	Th_{aq}	Ts_{halite}
Quartz veins									
Remnant crystals (crosscutting veins)									
Intra		G_1	−62.4/−56.6 (*41*)			−22.0/−2.2 (*48*)			
Intra	Immisc	G_1	−63.6/−56.6 (*41*)	−13.2/0.3 (*6*)		−27.7/28.9 (*91*)			
		W_1			n.m.[c]			decrep.[c]	239/248 (*4*)
Recrystallized grains (cementing and crosscutting veins)									
Intra		W_1			Not considered (imploded inclusions)				
Intra	Immisc	G_1	−58.7/−56.6 (*188*)	−12.5/−9.6 (*8*)		−20.7/28.4 (*229*)			
		(W_1)			−24.7/−24.0 (*8*)			decrep.[c]	
Inter	Immisc	G_2					L: −108.9/−81.2 (*54*) C: −85.2/−78.3 (*9*) V: −100.9/−80.4 (*49*)		
		W_2			−40.0/−32.3 (*5*)			47/129 (*12*)	n.m.[b]
Inter	Immisc	G_2					V: −88.0/−87.0 (*4*)		
		W_3			n.m.[c]			n.m.[c]	
Quartz globules									
Recrystallized grains									
Intra		W_1			Not considered (imploded inclusions)				
Intra	Immisc	G_2					L: −103.6/−84.7 (*160*) V: −108.0/−80.2 (*39*)		
		W_2			−39.2/−27.3 (*54*)			58/137 (*55*)	102/108 (*7*)
Inter	Immisc	G_2		5.9/18.4 (*16*)	−2.2/−0.1 (*11*)		V: −105.0/−94.8 (*10*)		
		W_3							

[a] "Intra", intragranular fluid inclusion assemblage; "Inter", intergranular fluid inclusion assemblage.
[b] Th_{CO_2} always to liquid, while the mode of homogenization of CH_4 is indicated with a letter (L, to liquid; C, by critical behaviour; V, to vapor).
[c] n.m., not measured; decrep., decrepitate before homogenization.

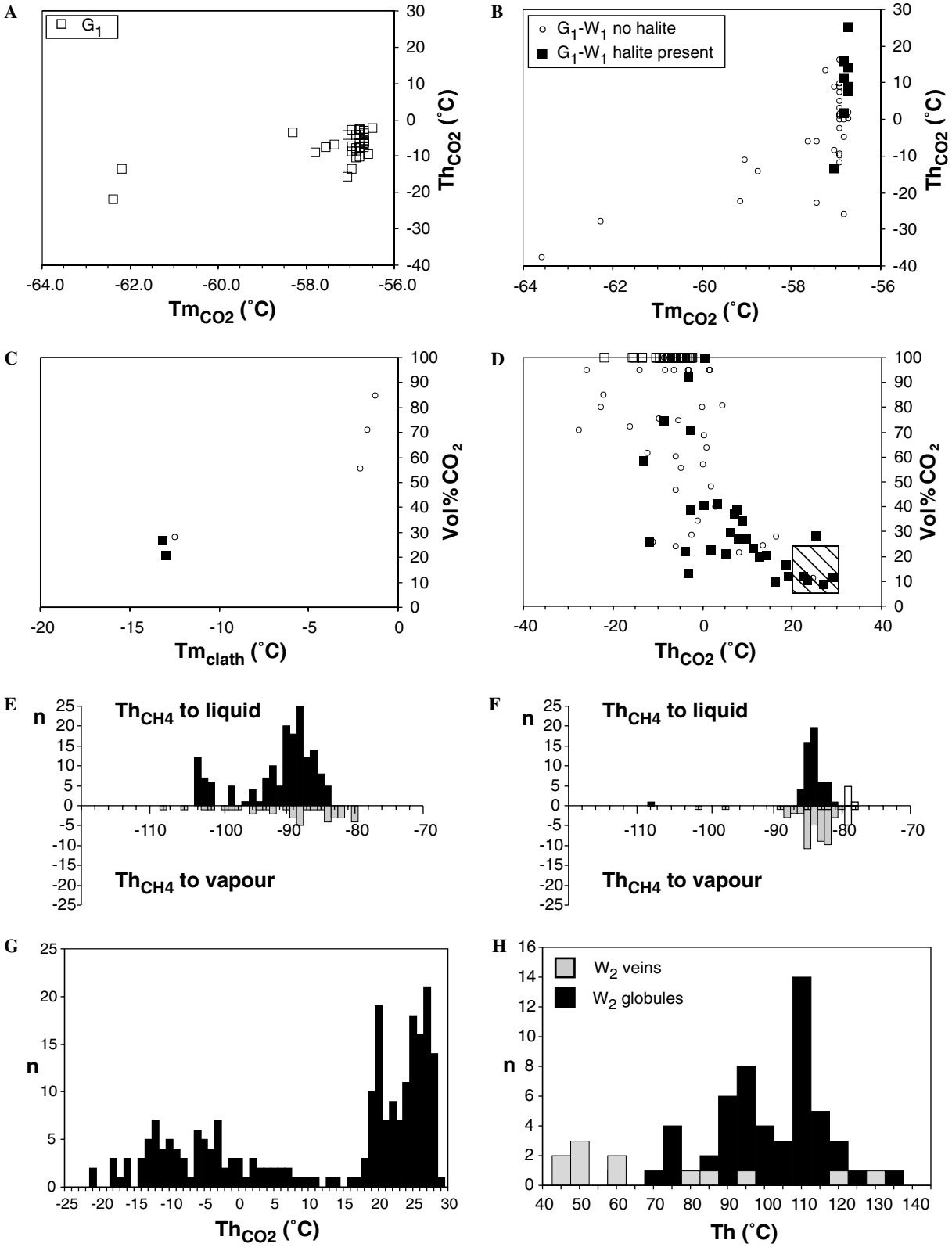

Fig. 5. Microthermometric measurements. (A) Tm_{CO_2} vs. Th_{CO_2} for G_1 inclusions in strained crystals in the quartz veins crosscutting the pillow breccia. (B) Tm_{CO_2} vs. Th_{CO_2} for gas- and aqueous-dominated inclusions in immiscible G_1–W_1 assemblages in crosscutting veins. (C) Tm_{clath} vs. vol% CO_2 in immiscible G_1–W_1 assemblages. Symbols are the same as in (B). (D) Th_{CO_2} vs. vol% CO_2 of inclusions in immiscible G_1–W_1 assemblages. Symbols are the same as in (A) and (B). (E, F) Histograms of Th_{CH_4} of $G_2^{L,C,V}$ inclusions in quartz globules (intragranular trails) and veins (intergranular trails), respectively. (G) Histogram of Th_{CO_2} of G_1 inclusions in intragranular trails in recrystallised grains of the cementing and crosscutting quartz veins. (H) Histogram of Th of W_2 inclusions in globules, and in cementing and crosscutting veins.

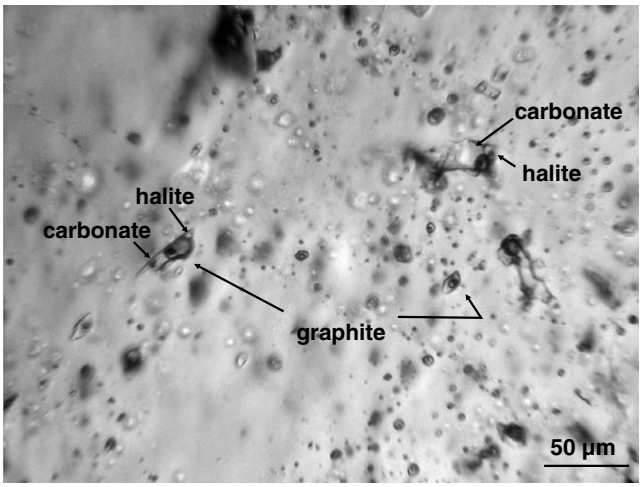

Fig. 6. Photograph showing an immiscible G_1–W_1 cluster in strained, remant crystals of the cementing quartz veins. Note the variable vol% of the gas and aqueous phases, the rounded, opaque graphite in the gas phase and the variable proportions of carbonate crystals in the aqueous phase.

Also, the inclusions from the former population have Tm_{CO2} right at the triple point of pure CO_2 (−56.6 °C), while this is typically 0.3° lower for inclusions of the latter population. Raman analyses demonstrated the presence of traces of CH_4 in inclusions from this latter population ($X_{CH_4} < 0.01$). When the intragranular trails intersect clusters of solid graphite in the grains, the graphite can be incorporated in an inclusion, but the microthermometric properties are identical to non graphite-bearing inclusions in the assemblage.

Urai et al. (1986), Drury and Urai (1990) and Johnson and Hollister (1995) suggested that during recrystallization aqueous fluids are preferentially removed, while CO_2-rich fluids are retrapped. Hollister (1990) suggest that trails of CO_2-rich inclusions can form due to transposition and H_2O-loss of grain-boundary fluids or fracture-related trails. However, as shown in Fig. 7, FIA's with consistent, but very different properties occur in the same individual crystal, and all of these contained sporadic aqueous dominated inclusions. Therefore, we believe it is not realistic to attribute the differences in Th_{CO_2} between such FIA's to preferential loss of an aqueous phase. Further, in contrast to G_1 inclusions in strained crystals, Tm_{CO2} and Raman analyses of inclusions in FIA's having lowest Th_{CO_2} (such as Trail 2 in Fig. 7), demonstrated that the lowest Th_{CO_2} is not due to the presence of CH_4, but indicates directly the molar volume of the CO_2-phase. We argue that the variation in molar volume between these populations are real and reflect different conditions of formation of G_1-dominated FIA's trapped along healed, intragranular fractures during and after the recrystallization process. Similar observations can be made in the recrystallized grains of the cementing veins, although fluid inclusions are less abundant. Also here, carbonate and some graphite are present as solid inclusions. Straight intragranular fluid inclusion trails contain G_1 and sporadically W_1 inclusions with identical variations in molar volume as found in the crosscutting veins. Molar volumes of the CO_2-phase can be calculated to range between 43.7 and 47.5 cm^3/mol in the first population (Fig. 5G), and between 53.6 and 74.1 cm^3/mol in the second population.

5.2.1.3. In recrystallized grains in quartz globules. Fluid inclusions in quartz globules in pillow fragments have already been described by Appel et al. (2001) and Touret (2003). Single aqueous, as well as gaseous inclusions occur sporadically in clusters with solid carbonate (and sometimes tourmaline) inclusions. Isolated gaseous inclusions appear very dark and contain low density methane (G_2^V). Although 36 wafers were investigated, all containing 20 or more globules, not a single CO_2-rich inclusion (G_1) was found. The aqueous inclusions frequently have a halite crystal, several solids and a gas bubble, in which Raman analyses of one inclusion detected the presence of CH_4. The size and abundance of different solids can vary widely, sometimes only leaving a small quantity of liquid and a deformed gas bubble. In the vicinity of the inclusions, there are often tiny (sub-µm) fluid inclusions creating a halo around inclusions. These features indicate that the fluid inclusions correspond to imploded, or even completely "collapsed" inclusions (Touret, 2001, 2003), similar to the isolated W_1 inclusions in the recrystallized grains of the cementing and crosscutting quartz veins. Two such inclusions showed Ts_{halite} of 118 and 361 °C (Th_{bub} of 194 and 172 °C, respectively). This indicates salinities of 28.5 and 37.1 eq. wt% NaCl (Sterner et al., 1988). Other solid phases did not dissolve on heating up to ~350 °C. Appel et al. (2001) and Touret (2003) reported isolated aqueous inclusions that are biphase but did not contain solid phases. Their reported Tm_{ice} ranged between −26.9 and −7.9 °C (Appel et al., 2001). In this study, only 3 such biphase inclusions were found in which ice was last to melt. Tm_{ice} varied between −23.8 and −17.1 °C.

Much more abundant (although still extremely rare compared to the amount of inclusions in the veins), are separated intragranular trails of either $G_2^{L,C,V}$ or W_2 inclusions. Inclusions are frequently somewhat relocated, indicating that recrystallization continued after formation of the FIA. An example of $G_2^{L,V}$ FIA's is given in Fig. 8. The separate trails in Fig. 8, have G_2 inclusions with distinctly different densities and X_{H_2}. All trails are associated with a relatively big calcite crystal and intergrown pyrrhotite. These minerals are located in the centre of a globule, but are fully contained within one perfectly recrystallized quartz crystal. All inclusions in Trail 1 homogenized to the liquid (G_2^L), while homogenization was to the vapor in Trails 2 and 3 (G_2^V). X_{H_2} for Trail 1 is 0.03, while it varies between 0.14 and 0.28 for Trails 2 and 3. Fig. 5E shows all measured Th_{CH_4} in FIA's made up of $G_2^{L,C,V}$ inclusions found in the samples investigated. For G_2^L inclusions this varied between −84.7 and −103.6 ($n = 160$). Th of all W_2

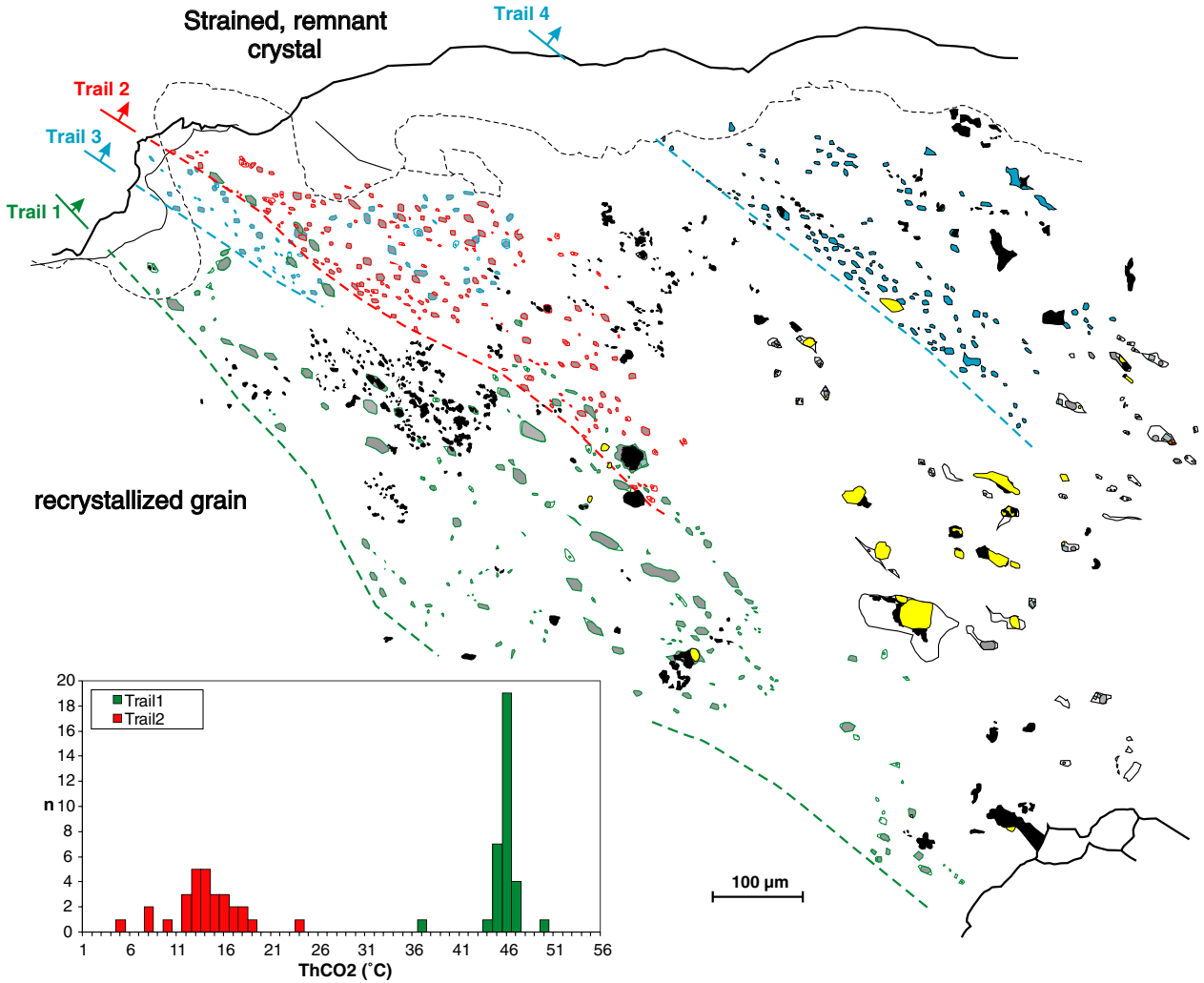

Fig. 7. Camera Lucida drawing of a recrystallized grain in the crosscutting quartz veins. Separate intragranular trails containing $G_1(-W_1)$ fluid inclusions are drawn in different colours. The histogram of Th_{CO_2} for Trail 1 and Trail 2 is shown in the inset. Thick solid line represents the grain boundary with a strained, remnant grain at top wafer surface, while hatched black line indicates the boundary at bottom surface. Yellow areas are carbonate crystals and black areas are highly ordered graphite. See text for discussion.

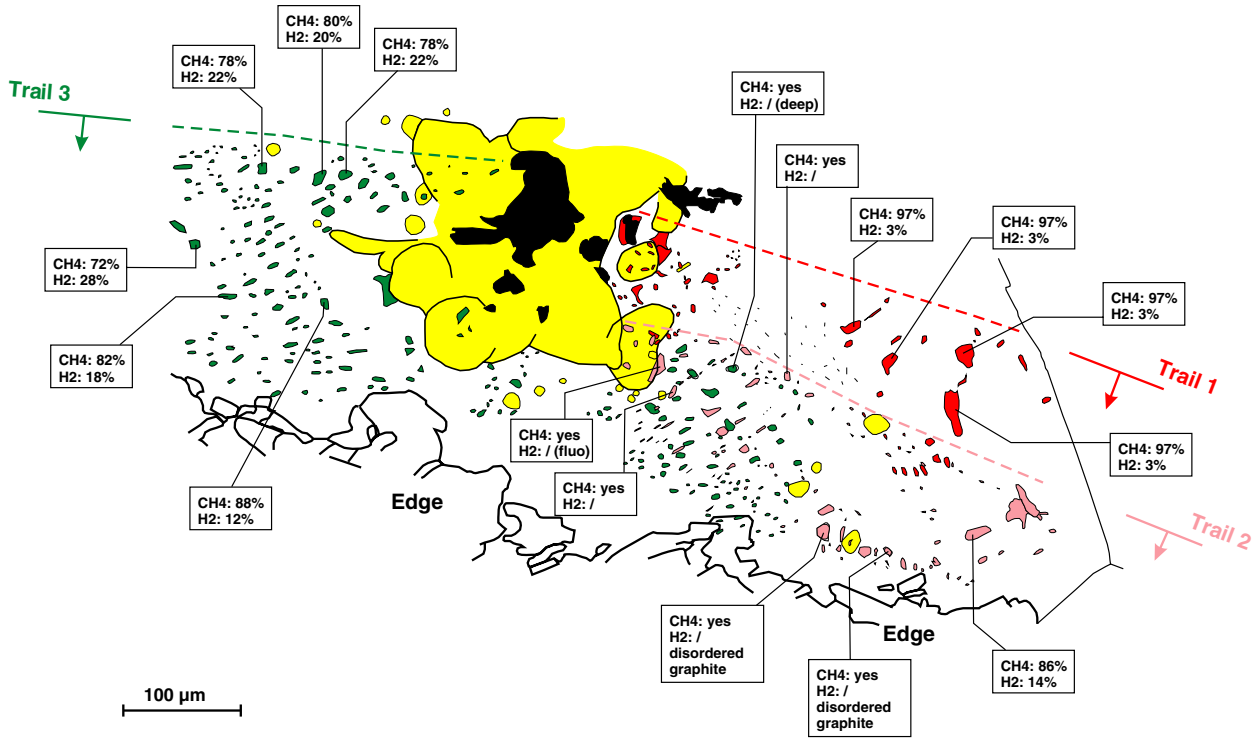

Fig. 8. (A, B) Transmitted (crossed polars) and reflected light photographs of a pillow fragment globule and its solid and fluid inclusion content. (C) Camera Lucida drawing of the large quartz grain in (A) and (B), showing three intragranular trails of G_2 inclusions. The central solids are calcite (yellow), pyrrhotite and Fe-oxides (black). Inclusions of Trail 1 all homogenizing to liquid (G_2^L). Trail 2 and 3 contain low- to critical density CH_4 (G_2^C and G_2^L). Yellow areas are solid carbonate inclusions located at variable depths. See text for discussion.

inclusions measured in the samples clusters around 90 to 120 °C (Fig. 5G; $n = 55$), whether or not associated with $G_2^{L,C,V}$ inclusions. In few cases where a halite crystal appeared after cryogenic runs, Tm_{halite} was around 105 °C (before Th_{tot}). This would correspond to a salinity of ~28 eq. wt% NaCl (Sterner et al., 1988).

5.2.2. Intergranular trails

5.2.2.1. Not visible using cathodoluminescence imaging. In the cementing and crosscutting quartz veins, intergranular trails not visible using cathodoluminescence imaging consist of either a gaseous or an aqueous component, but also mixed assemblages were found. However, in contrast to intragranular FIA's, the gaseous inclusions are $G_2^{(L,C,V)}$ inclusions, while the aqueous component is mostly made up of W_2 inclusions. Therefore, they are very similar to the *intra*granular FIA's found in the globules. A typical occurrence is given in Fig. 9 (cementing quartz vein). Note that between the different intergranular $G_2^{C,V}$ and W_2 trails shown in Fig. 9, some clustered and isolated G_1 and W_1 inclusions are present. G_2^L inclusions were also found as intergranular trails. The distribution of Th_{CH_4} of these high-density CH_4 inclusions is specific for each trail, but its total range is between −108.9 and −81.2 ($n = 54$). A summary of Th_{CH_4} for the different groups of inclusions (homogenizing to liquid, vapor or showing critical homogenization) is given in Fig. 5F. Interestingly, Raman analyses showed that methane inclusions with different densities have also distinguishable amounts of H_2. For G_2^L inclusions X_{H_2} varied between 0.02 and 0.04 ($n = 5$), while for G_2^V inclusions it varied between 0.06 and 0.16 ($n = 4$). The aqueous (W_2) inclusions in the intergranular assemblages were mostly monophase, but a gas bubble occasionally appeared after cryogenic measurements. If so, Th of the W_2 inclusions was between 47 and 129 °C ($n = 12$; Fig. 5H).

5.2.2.2. Visible (non-luminescent) using cathodoluminescence imaging. As shown in Fig. 3, some non-luminescent, healed intergranular fractures can be seen using SEM-CL, both in quartz veins (cementing and crosscutting) and in the globules in pillow fragments. In both cases they host mixed G_2^V and W_3 inclusions. W_3 inclusions are dominantly monophase, indicating a formation at temperatures lower then ~80 °C (Goldstein and Reynolds, 1994; Diamond, 2003b). When together with G_2^V inclusions in same FIA's, mixed inclusions have vol% of the gas phase varying between 5% and 90%, and Tm_{clath} in these inclusions was between 5.9 and 18.4 °C ($n = 16$). Th_{CH_4} of G_2^V inclusions varied between −105.0 and −87.0 °C ($n = 14$), but due to the difficulty of observation could well extend to lower values. Clearly, these G_2^V–W_3 FIA's represent the youngest fluid recorded in the samples. The sharp expression of the healed microfractures using SEM-CL indicates that they formed after quartz recovery.

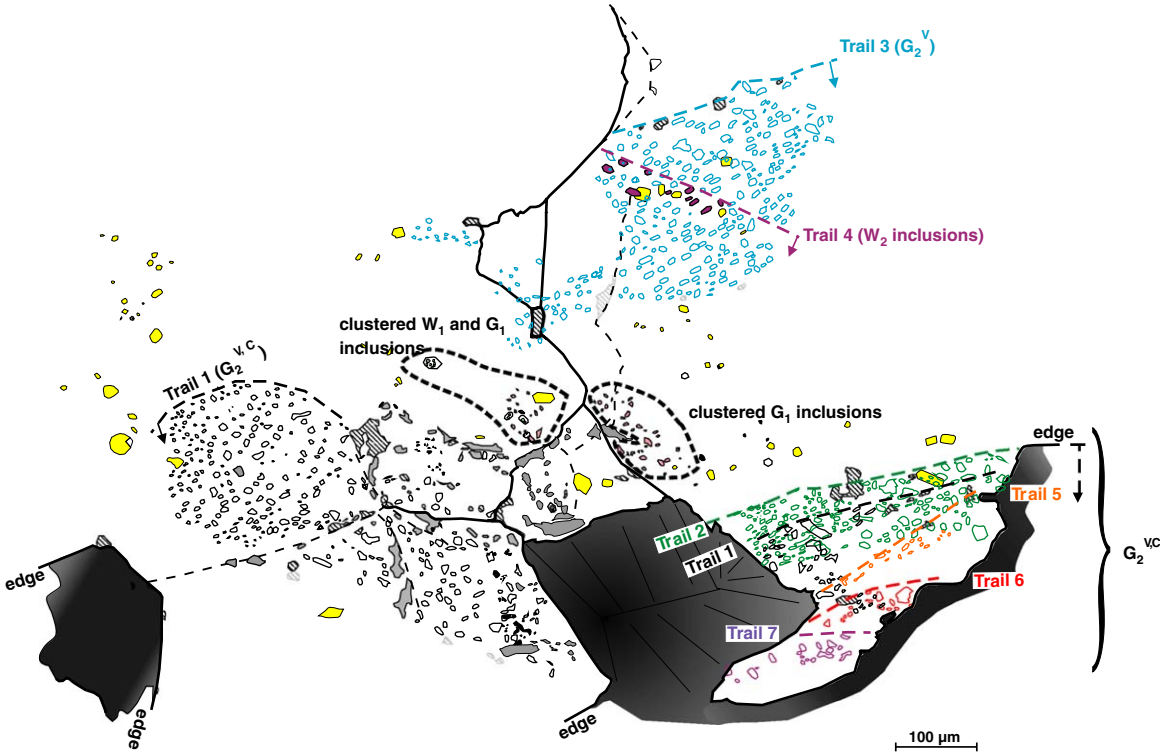

Fig. 9. Camera Lucida drawing of several unstrained vein quartz crystals (cementing vein) containing intergranular trails of $G_2^{C,V}$ inclusions. One trail (Trail 4) has biphase brine inclusions (W_2), and the solid carbonate inclusions (shown in yellow) also are located along this trail. Other carbonate inclusions are randomly distributed within the crystals (variable depths). Thick, full, black lines represent grain boundaries at top wafer surface, while thin, black, hatched lines indicate grain boundaries at bottom surface. See text for discussion.

In summary, the cementing and crosscutting quartz veins, and the quartz globules in pillow fragments have a remarkably different fluid inclusion content. The oldest fluid inclusions found in the crosscutting veins are present in remnant, strained crystals that survived complete recrystallization and they consist of CO_2-rich (+trapped graphite) (G_1) and halite-saturated, brine-rich (+CO_2, +trapped carbonate) (W_1) inclusions which form an equilibrium immiscible assemblage. Such inclusions were transposed or even completely wiped out in recrystallized grains. The recovery process was much more extensive in the earlier cementing veins, but the similarity in fluid and solid (carbonate, graphite) inclusion content suggest a similar origin. The recrystallized grains in both vein generations have younger FIA's trapped along *intra*granular trails which consist of CO_2-rich (G_1) or halite-saturated brine-rich (+CO_2) (W_1) inclusions. Moreover, the CO_2-rich assemblages show a bimodal density distribution. Still younger *inter*granular FIA's in both types of quartz veins have $CH_4 + H_2$ (with variable density) ($G_2^{L,C,V}$) or biphase brine inclusions (W_2) (Th $\sim$ 105 °C). Finally, the youngest fluid inclusions can be found along secondary, crosscutting, non-luminescent quartz that represents healed microfractures. They host low-density $CH_4 + H_2$ (G_2^V) and low-salinity aqueous inclusions (W_3) (Th $<\sim$ 80 °C). In contrast, in the quartz globules, no CO_2-bearing inclusions were found. The oldest fluid inclusions in these quartz segregations could be isolated, collapsed halite saturated brine (+carbonate) inclusions (W_1). However, most abundant in the globules are *intra*granular FIA's consisting of $CH_4 + H_2$ (variable density) ($G_2^{L,C,V}$) and/or biphase brine inclusions (W_2) (Th $\sim$ 105 °C). As for the veins, the youngest fluid inclusions are found along non-luminescent, healed fractures and consist of low-density $CH_4 + H_2$ (G_2^V) and low-salinity aqueous inclusions (W_3) (Th $<\sim$80 °C).

6. Discussion

6.1. Fluid inclusions in the pillow fragment globules: remnants of an early seafloor-hydrothermal system or retrograde metamorphic fluids?

Appel et al. (2001) suggested that the globules in the pillow fragments were formed during, or shortly after, submarine eruption and persisted throughout the subsequent rock history. Similar textures can be found in both modern and ancient pillow basalts (e.g. Wilson, 1989; Waters and Wallace, 1992; Barley, 1993), where amygdules are filled with silica- or carbonate-rich mineralogy. Here, they correspond to former gas vesicles trapped in an ascending (boiling) magma. The spherical shape can be preserved if they are filled early after magma eruption, possibly during seafloor-hydrothermal alteration (Alt, 1995; Nakamura and Katu, 2004). This similarity between the globules in the pillow breccia fragments and present-day equivalents, led Appel et al. (1998), to suggest an origin as cemented gas vesicles. However, it is difficult to conclude whether the quartz itself (as found today) is primary, or whether it replaced pre-existing silica- or carbonate-rich mineralogy, because all crosscutting relations are obliterated by the recrystallization process.

A new find of this study is the presence of $CH_4 + H_2$ (G_2) and associated highly saline brine (W_2) inclusions as intergranular fluid inclusion trails in the quartz veins, either cementing or crosscutting the pillow lava breccia. This indicates that such immiscible fluids were present in the late stages of quartz recrystallization, and therefore during the retrograde metamorphic evolution. It sheds new light on the occurrence of similar fluid inclusions in the pillow fragment globules (Appel et al., 2001; Touret, 2003). In the globules, such fluid inclusions are present either isolated, clustered or, more frequently, as intragranular trails fully contained within individual crystals. However, the microfabric of the quartz veins and quartz globules suggests that recrystallization was much more prominent in the latter. Also, the recrystallization mechanisms seem to have been different, with dynamic recrystallization being dominant in the vein quartz while static processes prevailed in the quartz globules. As discussed by Appel et al. (2001) this could be due to the difference in competence between the altered matrix and the quartz globules, causing most strain to be taken up by the matrix. In either case, from a fluid inclusion point of view, both recrystallization processes can lead to transposition, reequilibration and obliteration of fluid inclusion assemblages (e.g. Kerrich, 1976; Wilkins and Barkas, 1978; Urai et al., 1986; Bouiller et al., 1989; Drury and Urai, 1990; Johnson and Hollister, 1995). Originally, the *intra*granular trails and clusters found in the quartz globules, could have been formed as *inter*granular healed fractures, broken up and transposed in the recovering quartz host.

In addition, cathodoluminescence imaging showed that, both in the veins and the globules, low-density G_2^V–W_3 inclusions are the latest FIA's formed, since they occur in non-luminescent microfractures. This provides evidence that methane-rich fluids were present late in the metamorphic evolution. As Raman analyses showed that the G_2 inclusions contain a significant X_{H_2}, it could be suspected that hydrogen diffusion through the quartz host altered the composition of any early CO_2 inclusions that would have been present. From natural examples and experiment, hydrogen diffusion through quartz seem to be very fast at temperatures >500 °C (Hall and Bodnar, 1990; Hall et al., 1991a,b; Morgan et al., 1993; Mavrogenes and Bodnar, 1994; Pasteris and Chou, 1998). However, the ubiquitous presence of CO_2-rich FIA's in zones dominated by high- and low-density, hydrogen-bearing G_2 inclusions in the quartz veins (e.g. Fig. 10) suggest that this process was negligible in the pillow breccia occurrence. As a consequence, this indicates that the vein (and globule) quartz was closed to hydrogen diffusion at

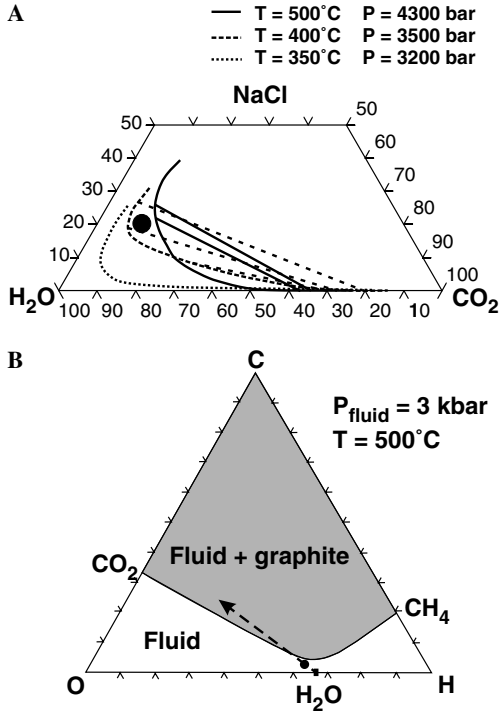

Fig. 10. (A) Ternary diagram for the H_2O–CO_2–NaCl system, showing the immiscibility boundaries at different P and T (calculated using the EOS of Duan et al., 1995, 2003). Tie-lines connect coexisting liquid and vapor phases. The full circle represents the approximated composition of the liquid end-member fluid of G_1–W_1 inclusions in strained, remnant vein crystals as deduced from Fig. 5D. (B) Explanatory ternary C–O–H diagram showing the graphite saturation boundary at a randomly chosen P and T (after Huizenga, 2001). A graphite undersaturated fluid with arbitrary composition (block dot) could move into the graphite field by loss of H_2O (indicated by arrow).

the time that such $CH_4 + H_2$ fluids were present in the rock porosity. A closure temperature for hydrogen diffusion through quartz is not precisely known, but the process does not appear to be significant below 200–300 °C (Morgan et al., 1993).

We conclude that fluid inclusion assemblages found in the globules are retrograde fluids, not remnants of an early seafloor-hydrothermal system. We also suggest that the difference in fluid inclusion content between globules, cementing and crosscutting veins (i.e. CH_4 vs. CO_2-dominated) reflects the extent of recovery processes. In other words, all earlier fluid inclusions have been wiped out in the globule quartz and only the latest fluids trapped remain.

6.2. Fluid immiscibility, P–T evolution and fluid flow evolution

6.2.1. FIA's in remnant, strained crystals of the crosscutting quartz veins

Having cleared the late timing of formation of G_2–W_2 inclusions, the oldest unaltered FIA's still found at the pillow breccia locality are the assemblages in the remnant strained crystals of the crosscutting quartz veins. Their microthermometric properties indicate that they represent products of an equilibrium immiscibility process of an original, homogeneous H_2O–CO_2-(CH_4)–salt fluid. Moreover, it appears that carbonates and graphite were trapped in the liquid and vapor endmember, respectively (Fig. 6). The nature of salts present in the aqueous phase is unknown, but the presence of halite suggests that NaCl is a major contributor. When simplified to an H_2O–CO_2–NaCl system, a ternary phase diagram (Fig. 10A; Pichavant et al., 1982; Duan et al., 1995, 2003) predicts that in a large range of *P–T* conditions, equilibrium immiscibility leads to a liquid endmember enriched in salts and H_2O, but depleted in CO_2 relative to the parent fluid. Carbonate precipitation in the liquid endmember could have been induced by this CO_2 depletion. The resulting vapor endmember, on the other hand, is strongly depleted in salts, depleted in H_2O and enriched in CO_2 relative to the parent fluid. In a C–O–H diagram (Fig. 10B), it can be seen that H_2O depletion can lead to graphite saturation of an original undersaturated fluid. Therefore, carbonate and graphite precipitation could have occurred simultaneously from endmember fluid phases as an indirect consequence of the immiscibility process. Although the chemical activity of all fluid components in the endmember fluids would initially be the same after phase separation, this process creates physically separated fluids that respond differently to the local physico-chemical conditions. The X_{CO_2}/X_{CH_4} of the parent fluid is difficult to estimate, but possibly, the sporadically higher presence of CH_4 in G_1 inclusions (Figs. 5A, B) could be a metastable remnant of the immiscibility process (e.g. Huizenga and Touret, 1999). It was argued above that such a sporadic higher X_{CH_4} does not correspond to a lower molar volume of the inclusions, again ruling out the possibility of resetting due to H_2 exchange (Dubessy, 1984; Cesare, 1995).

Ideally, in the case of equilibrium immiscibility, Th_{tot} of the endmember fluid inclusions would equal the trapping *P–T* conditions (Pichavant et al., 1982; Roedder, 1984; Diamond, 2003a), but unfortunately, Th_{tot} could not be measured because both gaseous and liquid endmember fluids decrepitate prior to homogenization. However, since gaseous endmember fluids only have a small aqueous phase (probably not exceeding ~10 vol%), their isochores can be approached by treating them as pure CO_2 inclusions (for Th_{CO_2} between −10 and −0 °C; molar volume between 44.8 and 47.5 cm^3/mol). True isochores would have a slightly steeper slope in *P–T* space. For the aqueous-dominated endmember fluid, its composition could be estimated from Fig. 5D. If one considers Th_{CO_2} to vary between 20 and 30 °C, volume CO_2 between 5% and 25%, volume halite to be 10%, and taking a salinity between 30 and 33 eq. wt% NaCl, the calculated composition would have X_{H_2O} between 0.74 and 0.66, X_{CO_2} between 0.06 and 0.14, and X_{NaCl} between 0.19 and 0.20, respectively. The range of solvi is shown in Fig. 11. These solvi were calculated with the program GEOFLUIDS, programmed by Z. Duan, N. Møller and J.H. Weare (website: geotherm.ucsd.edu) using the Equation of State (EOS) of Duan et al. (1995, 2003).

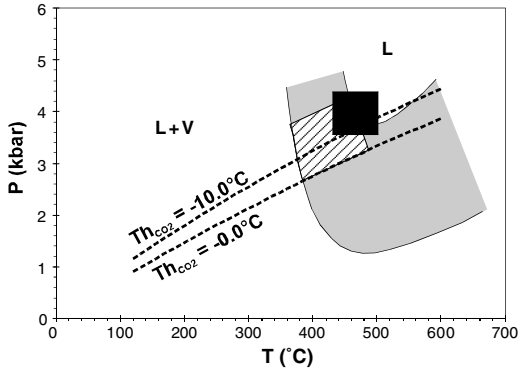

Fig. 11. *P–T* diagram showing the range of solvi (in grey) of the H_2O–CO_2–NaCl system for an aqueous endmember fluid (calculated using the EOS of Duan et al., (1995, 2003). Also shown are two isochores for pure CO_2 inclusions with Th of −10.0 and 0.0 °C. The presence of an aqueous phase in such inclusions would shift the isochores to higher pressures. Preferred trapping conditions of immiscible assemblages found in the strained, remnant crystals in crosscutting quartz veins are indicated by the hatched box. Black box delineates peak-metamorphic conditions for the pillow breccia outcrop (Appel et al., 2001).

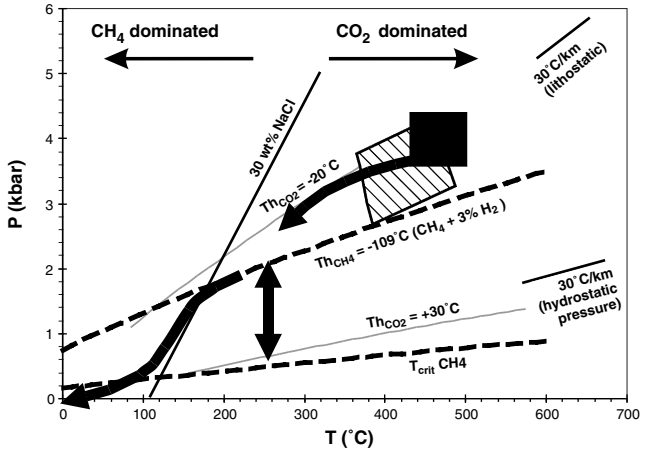

Fig. 12. *P–T* diagram showing boundary conditions for the post-metamorphic evolution of the pillow breccia outcrop, as derived from fluid inclusions. Indicated are trends for geothermal gradients for 10 and 30 °C/km under lithostatic pressures, and for 30 °C under hydrostatic pressures. See text for discussion.

Experimental data on the H_2O–NaCl–CO_2 system at elevated salinities (Schmidt and Bodnar, 2000) could suggest that the EOS of Duan et al. (1995, 2003) is less accurate for salinities ~20 to 40 wt% NaCl. However, comparison of Figs. 6 and 7 of Schmidt and Bodnar (2000) suggests that using the EOS of Duan et al. (1995, 2003) would lead to errors probably less than 50 °C. This would not influence our conclusions significantly. Combining the isochores of the gaseous endmember fluids (minimum slopes) and the range in possible solvi of the immiscibility field for the aqueous endmember, preferred *P–T* conditions for the immiscibility process and the trapping of the FIA's found in remnant, strained crystals in the crosscutting veins, would be 370–480 °C at pressures of 2.7–4.2 kbar (Fig. 11). The higher end of this *P–T* range overlaps with the peak-metamorphic conditions derived for the locality from mineral composition and garnet–biotite geothermometry (Appel et al., 2001). This indicates that immiscibility, carbonate and graphite crystallization and fluid inclusion formation occurred at or near peak-metamorphic conditions.

6.2.2. Post peak-metamorphic P–T evolution

The intragranular G_1 and W_1 FIA's in recrystallized vein crystals could also represent immiscible trapping. However, in contrast to the remnant, strained crystals, no clear mixed assemblages were found, which makes it difficult to decide on whether the processes of equilibrium immiscibility, mixing of heterogeneous fluids or recycling and refinement of pre-existing heterogeneous FIA's (e.g. Johnson and Hollister, 1995) are dominant. This is equally true for assemblages in later, intergranular trails. We therefore focus solely on the carbonic, gaseous intragranular FIA's in recrystallized vein crystals which document consistent differences in molar volume. Fig. 12 shows isochores for inclusions having Th_{CO_2} of −20 and +30 °C, representative for the lowest and highest molar volume of intragranular G_1 FIA's (42.7 and 74.1 cm^3/mol, respectively). We argued above that high-density, *inter*granular $CH_4 + H_2$ (G_2) inclusions were formed at temperatures below ~200–300 °C, since no hydrogen diffusion seems to have occurred. Nevertheless, they have volumetric properties which indicate higher pressures then recorded by the lowest density G_1 FIA's in intragranular trails. The difference between the lowest density G_1 inclusions and highest density G_2 inclusions therefore does indeed require important changes in pressure, although perhaps at relatively low temperatures (Fig. 12). Possibly, this change in pressure is due to variations in fluid pressure during the introduction of G_2–W_2 fluids at the pillow breccia locality.

A last constraint on the retrograde *P–T* evolution is given by the isochores for the W_2 inclusions which show a Th clustered around 105 °C, and the G_2^V–W_3 FIA's in non-luminescent, healed microfractures, which formed below ~80 °C. Based on these fluid inclusion constraints, a preferred retrograde *P–T* evolution of the pillow breccia occurrence is given in Fig. 12. With the exception of the pressure variations discussed above it would be close to a normal geothermal gradient of 30 °C/km.

6.3. Evolution of the redox state and the composition of the carbonic phase

In all quartz segregations at the pillow breccia occurrence, either CO_2-dominated (G_1) or CH_4-dominated (G_2) carbonic fluids were found. No intermediate mixtures seem to be present. This is in agreement with the expected speciation in a graphite-bearing system C–H–O system, because at $T < 500$ °C, the graphite stability field essentially coincides with the CO_2–H_2O and CH_4–H_2O binaries in a C–O–H diagram (Fig. 10B; Holloway, 1984; Huizenga, 2001). We follow Giggenbach (1987) in that the

$\log f_{H_2}/f_{H_2O}$ is a more useful parameter to describe the redox conditions of the fluids at $T < 600$ °C, then the "theoretical" $\log f_{O_2}$. In a C–O–H system, the main equilibria governing speciations of C–O–H species can then be written as (Ohmoto and Kerrick, 1977; Huizenga, 2001)

$$CH_4 + 2H_2O = CO_2 + 4H_2 \quad (1)$$

and

$$C + 2H_2O = CO_2 + 2H_2 \quad (2)$$

Log f_{H_2}/f_{H_2O} can be calculated when X_{CH_4}/X_{CO_2} or X_{H_2}/X_{CH_4} is known, and considering that $X_{H2O} + X_{CO_2} + X_{CH_4} + X_{H_2} = 1$. For a fluid in equilibrium with graphite (carbon activity in the fluid phase is 1) at 450 °C and 4 kbar, having $X_{CH_4}/X_{CO_2} = 0.01$, the calculated f_{H_2}/f_{H_2O} is −2.39 (Fig. 13), which is very close to the Quartz–Fayalite–Magnetite (QFM) buffer, and only slightly more reducing than the Biotite–Almandine–Muscovite–Magnetite (BAMM) buffer (Zen, 1985). The BAMM buffer curve shown in Fig. 13 was calculated using the composition of biotite, garnets and muscovite from the pillow breccia occurrence, analyzed by microprobe (Rollinson, pers. comm.), but since ilmenite is present in the pillow fragment matrix instead of magnetite, the calculated BAMM would be more oxidizing than the actual host rock. Also, the addition of salts to the fluid system would reduce the activity of H_2O and would increase the calculated value of $\log f_{H_2}/f_{H_2O}$. Despite these uncertainties, the composition of the carbonic phase seems to be in agreement with a rock-buffered fluid system at peak-metamorphic conditions.

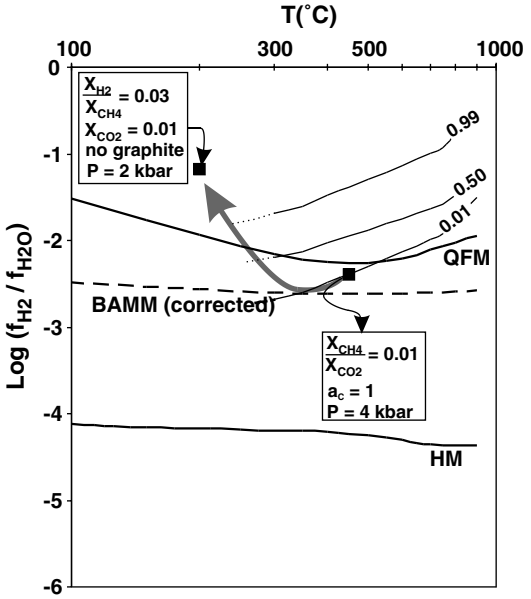

Fig. 13. $\log f_{H_2}/f_{H_2O}$ vs. temperature. Calculated $\log f_{H_2}/f_{H_2O}$ for a graphite-saturated fluid at 450 °C and 4 kbar, having $X_{CH_4}/X_{CO_2} = 0.01$ is close to the Quartz–Fayalite–Magnetite (QFM) and corrected Biotite–Almandine–Muscovite–Magnetite (BAMM; Zen, 1985) buffers (at 4 kbar), while G_2–W_2 fluids at 200 °C and 2 kbar indicate much more reducing conditions and disequilibrium with graphite. Also shown is the Hematite–Magnetite (HM) buffer and predominance boundaries for $X_{CH_4}/X_{CO_2} = 0.01, 0.5$ and 0.99 in graphitic systems at 4 kbar.

However, an evolution towards a carbonic fluid having $X_{CO_2}/X_{CH_4} < 0.01$ and $X_{H_2}/X_{CH_4} \sim 0.03$ at 200 °C and 2 kbar, as deduced from the retrograde P–T evolution, requires $a_C < 1$. This indicates disequilibrium with graphite at these low temperatures. A blocking temperature for the H_2O–CO_2–CH_4–graphite system could be ~370 °C (Ramboz et al., 1985). Moreover, using only Eq. 1, the calculated $\log f_{H_2}/f_{H_2O}$ would be −1.18, which is significantly below the QFM or BAMM buffers. This suggests that the reducing, and immiscible G_2 and W_2 fluids are exotic to the breccia occurrence. In the entire IGB, meter- to kilometer-sized lenses of serpentinite and/or anthophyllite-rich ultramafic rocks are present (Rosing and Rose, 1993; Rose et al., 1996; Myers, 2002). Possibly, serpentinization or deserpentinization of these rocks during retrograde metamorphism controlled the formation of the reducing fluids (e.g. Coveney et al., 1987; Peretti et al., 1992; Orione et al., 2003). Moreover, the volumetric properties of the successive FIA's suggest fluid pressure variations accompanied the introduction of such reducing fluids at temperatures <~200 °C.

6.4. Significance of graphite

From the observation that graphite was trapped in CO_2-rich fluid inclusions at or near peak-metamorphic conditions, it follows that at this locality, the origin of graphite is by inorganic deposition from a fluid phase at or near peak-metamorphic conditions. Its later distribution as solid inclusions in the quartz grains is due to recrystallization and the resulting destruction of the fluid inclusions and removal of the fluid component. Such an origin of graphite microparticles has been proposed previously (Naraoka et al., 1996), but has never been proven. In an extensive study of graphite occurrence in the IGB, Van Zuilen et al. (2002, 2003) concluded that most graphite formed due to disproportionation of siderite, given its close association with siderite and magnetite. While this might be the dominant mechanism of graphite formation in the IGB, this study shows that at the pillow breccia occurrence, graphite and carbonate microcrystals in the recrystallized rocks originated by cogenetic deposition from a fluid phase.

7. Conclusions

The supracrustal lithologies of the Isua Greenstone Belt contain some of the oldest, well-preserved Early Archean rocks on Earth and potentially provide information on the nature of the earliest hydrosphere. However, the Isua rocks were affected by several fluid flow events and by metamorphism. In this study, we argue that recrystallization obliterated all fluid inclusion evidence of early sea-floor-hydrothermal processes at a weakly deformed pillow lava breccia occurrence in the least altered northeastern part of the belt, and that the oldest unaltered inclu-

sions that can still be found here were formed at or near peak-metamorphic conditions (~460 °C and ~4 kbar). These fluid inclusions are preserved in remnant, strained crystals of the quartz veins crosscutting the pillow breccia, and contain an immiscible assemblage of CO_2-rich (+trapped graphite) and brine-rich (+trapped carbonate) fluids. Their occurrence and compositional and volumetric properties suggest that they were formed during equilibrium immiscibility of an original homogeneous H_2O–CO_2–(CH_4)–NaCl(–other salt) fluid, and that graphite and carbonate were precipitated cogenetically from physically separated end-member fluids.

Inclusions trapped along intragranular trails in recrystallized quartz grains mainly contain separated CO_2(–H_2O) and highly saline H_2O–CO_2–NaCl(–other salt) fluids which were trapped at successive *P–T* conditions during retrograde evolution that was close to a lithostatic geothermal gradient of 30 °C/km. Strongly reduced CH_4–H_2 fluids (X_{H_2} up to 0.3) and immiscible, highly saline, metastable H_2O–NaCl(–other salt?) fluid inclusions are present along late, intergranular trails in the breccia cementing and crosscutting veins, but are located in intragranular or clustered assemblages in quartz globules in the pillow fragments. They were introduced at the breccia occurrence at temperatures <300 °C and their lower molar volumes in comparison with previous CO_2-rich inclusions, indicates variations in fluid pressure, likely between ~200–300 °C and 0.5–2 kbar.

Modeling the oxidation state in a H_2O–CO_2–CH_4– H_2–graphite system suggests that the fluids were buffered by local equilibrium with the host rock at peak-metamorphic conditions, but became much more reducing at low temperatures, probably due to external control by ultramafic lithologies in the IGB.

Finally, this study shows that microscopic graphite particles in recrystallized quartz grains in the IGB can be deposited inorganically from a fluid phase, adding to the complexity of processes that controlled the origin of reduced carbon in these Early Archean rocks.

Acknowledgments

The manuscript benefitted from constructive reviews by J.-M. Huizenga, L.S. Hollister, an anonymous reviewer and the editorial editor R.C. Burruss, which are gratefully acknowledged. We thank Ph. Muchez, D.A. Banks, H. Rollinson and B.W.D. Yardley for aid and comments during the course of the research. This study is part of the Isua Multidisciplinary Research Project funded partly by the Danish Natural Science Research Council. The first author's work was funded through a Post Doc. fellowship from the Danish Natural Science Research Council. The article is published with the permission of the Geological Survey of Denmark and Greenland.

Associate editor: Robert C. Burruss

References

Alt, J.C., 1995. Subseafloor processes in mid-ocean ridge hydrothermal systems. In: Humphris, S.E., Zierenberg, R., Mullineaux, L., Thomson, R. (Eds.), *Seafloor Hydrothermal Systems: Physical, Chemical, Biological and Geological Interactions within Hydrothermal Systems*. *Geophysical Monographs*, **91**, 85–114.

Appel, P.W.U., Fedo, C.M., Moorbath, S., Myers, J.S., 1998. Recognizable primary volcanic and sedimentary features in a low-strain domain of the highly deformed, oldest known (~3.7–3.8 Gyr) greenstone belt, Isua, West Greenland. *Terra Nova* **10**, 57–62.

Appel, P.W.U., Rollinson, H.R., Touret, J.L.R., 2001. Remnants of an Early Archean (>3.75 Ga) sea-floor, hydrothermal system in the Isua Greenstone Belt. *Precamb. Res.* **112**, 27–49.

Audétat, A., Günther, D., 1999. Mobility and H_2O loss from fluid inclusions in natural quartz crystals. *Contrib. Mineral. Petrol.* **137**, 1–14.

Bakker, R.J., Brown, P.E., 2003. Computer modeling in fluid inclusion research. In: Samson, I., Anderson, A., Marshall, D. (Eds.), *Fluid Inclusions: Analysis and Interpretation*. *Mineral. Ass. Can. Short Course* **32**, 175–212.

Bakker, R.J., 2003. Package FLUIDS 1. Computer programs for analysis of fluid inclusion data and for modeling bulk fluid properties. *Chem. Geol.* **194**, 3–23.

Bakker, R.J., Jansen, J.B.H., 1990. Preferential water leakage from fluid inclusions by means of mobile dislocations. *Nature* **345**, 58–60.

Bakker, R.J., Jansen, J.B.H., 1991. Experimental post-entrapment water loss from synthetic CO_2–H_2O inclusions in natural quartz. *Geochim. Cosmochim. Acta* **55**, 2215–2230.

Barley, M.E., 1993. Volcanic, sedimentary and tectonostratigraphic environments of the 3.46 Ga Warrawoona Megasequence: a review. *Precamb. Res.* **60**, 47–67.

Boak, J.L., Dymek, R.F., 1982. Metamorphism of the ca. 3800 Ma supracrustal rocks at Isua, West Greenland: implications for early Archean crustal evolution. *Earth Planet. Sci. Lett.* **59**, 155–176.

Bouiller, A.M., Michot, G., Pecher, A., Barres, O., 1989. Diffusion and/or plastic deformation around fluid inclusions in synthetic quartz: new investigations. In: Bridgewater, D. (Ed.), *Fluid Movements—Element Transport and the Composition of the Deep Crust*. Kluwer Academic Publishers, pp. 345–360.

Cesare, B., 1995. Graphite precipitation in C–O–H fluid inclusions: closed system compositional and density changes, and thermobarometric implications. *Contrib. Mineral. Petrol.* **122**, 25–33.

Channer, D.M.DeR., de Ronde, C.E.J., Spooner, E.T.C., 1997. The Cl^-–Br^-–I^- composition of ~3.23 Ga modified seawater: implications for the geological evolution of ocean halide chemistry. *Earth Planet. Sci. Lett.* **150**, 325–335.

Coveney Jr., R.M., Goebel, E.D., Zeller, E.J., Dreschhoff, G.A.M., Agino, E.E., 1987. Serpentinization and the origin of hydrogen gas in Kansas. *Am. Ass. Petroleum Geol. Bull.* **71**, 39–48.

Crowley, J.L., 2003. U-Pb geochronology of 3810–3630 Ma granitoid rocks south of the Isua greenstone belt, southern West Greenland. *Precamb. Res.* **126**, 235–257.

De Ronde, C.E.J., Channer, D.M.DeR., Faure, K., Bray, C.J., Spooner, E.T.C., 1997. Fluid chemistry of Archean seafloor vents: implications for the composition of circa 3.2 Ga seawater. *Geochim. Cosmochim. Acta* **61**, 4025–4042.

Diamond, L.W., 1992. Stability of CO_2 clathrate hydrate + CO_2 liquid + CO_2 vapor + aqueous KCl–NaCl solutions: experimental determination and application to salinity estimates of fluid inclusions. *Geochim. Cosmochim. Acta* **56**, 273–280.

Diamond, L.W., 2003a. Introduction to gas-bearing, aqueous fluid inclusions. In: Samson, I., Anderson, A., Marshall, D. (Eds.), *Fluid Inclusions: Analysis and Interpretation*. *Mineral. Ass. Can. Short Course* **32**, 101–158.

Diamond, L.W., 2003b. Systematics of H_2O inclusions. In: Samson, I., Anderson, A., Marshall, D. (Eds.) *Fluid Inclusions: Analysis and Interpretation*. Mineral. Ass. Can. Short Course **32**, 55–79.

Drury, M.R., Urai, J.L., 1990. Deformation-related recrystallization processes. *Tectonophysics* **172**, 235–253.

Duan, Z., Møller, N., Weare, J.H., 1995. Equation of state for the NaCl–H_2O–CO_2 system: prediction of phase equilibria and volumetric properties. *Geochim. Cosmochim. Acta* **59**, 2869–2882.

Duan, Z., Møller, N., Weare, J.H., 2003. Equations of state for the NaCl–H_2O–CH_4 system and the NaCl–H_2O–CO_2–CH_4 system: phase equilibria and volumetric properties above 573 K. *Geochim. Cosmochim. Acta* **67**, 671–680.

Dubessy, J., 1984. Simulation des équilibres chimiques dans le système C–O–H. Conséquences méthodologiques pour les inclusions fluides. *Bull. Minéral.* **107**, 155–168.

Foriel, J., Philippot, P., Rey, P., Somogyi, A., Banks, D., Ménez, B., 2004. Biological control of Cl/Br and low sulfate concentration in a 3.5-Gyr-old seawater from North Pole, Western Australia. *Earth Planet. Sci Lett.* **228**, 451–463.

Frei, R., Rosing, M.T., Waight, T.E., Ulfbeck, D.G., 2002. Hydrothermal-metasomatic and tectono-metamorphic processes in the Isua supracrustal belt (West Greenland): a multi-isotopic investigation of their effects on the Earth's oldest oceanic crustal sequence. *Geochim. Cosmochim. Acta* **66**, 467–486.

Friend, C.L.R., Nutman, A.P., 2005. New pieces to the Archean terrane jigsaw puzzle in the Nuuk region, southern West Greenland: steps in transforming a simple insight in a complex regional tectonothermal model. *J. Geol. Soc. London* **164**, 147–162.

Friend, C.R.L., Nutman, A.P., Baadsgaard, H., Kinny, P.D., McGregor, V.R., 1996. Timing of late Archeaen terrane assembly, crustal thickening and granite emplacement in the Nuuk region, southern West Greenland. *Earth Planet. Sci. Lett.* **142**, 353–365.

Giggenbach, W.F., 1987. Redox processes governing the chemistry of fumarolic gas discharges from White Island, New Zealand. *Appl. Geochem.* **2**, 143–161.

Goldstein, R.H., Reynolds, T.J., 1994. Systematics of Fluid Inclusions in Diagenetic Minerals. *SEPM Short Course* **31**, 199.

Gruau, G., Rosing, M., Bridgewater, D., Gill, R.C.O., 1996. Resetting of Sm–Nd systematics during metamorphism of >3.7 Ga rocks: implications for isotopic models of early Earth differentiation. *Chem. Geol.* **133**, 225–240.

Hall, D.L., Bodnar, R.J., 1990. Methane in fluid inclusions from granulites: a product of hydrogen diffusion? *Geochim. Cosmochim. Acta* **54**, 641–651.

Hall, D.L., Bodnar, R.J., Craig, J.R., 1991a. Fluid inclusion constraints on the uplift history of the metamorphosed massive sulphide deposits at Ducktown, Tennessee. *J. Metamorphic Geol.* **9**, 551–565.

Hall, D.L., Bodnar, R.J., Craig, J.R., 1991b. Evidence for postentrapment diffusion of hydrogen into peak metamorphic fluid inclusions from the massive sulphide deposits at Ducktown, Tennessee. *Am. Miner.* **76**, 1344–1355.

Hayashi, M., Komiya, T., Nakamura, Y., Maruyama, S., 2000. Archean regional metamorphism of the Isua supracrustal belt, southern West Greenland: implications for a driving force for Archean plate tectonics. *Int. Geol. Rev.* **42**, 1055–1115.

Hirth, G., Tullis, J., 1992. Dislocation creep regimes in quartz aggregates. *J. Struct. Geol.* **14**, 145–159.

Hollister, L.S., 1990. Enrichment of CO_2 in fluid inclusions in quartz by removal of H_2O during crystal-plastic deformation. *J. Struct. Geol.* **12**, 895–901.

Holloway, J.R., 1984. Graphite–CH_4–H_2O–CO_2 equilibria at low-grade metamorphic conditions. *Geology* **12**, 455–458.

Huizenga, J.M., 2001. Thermodynamic modeling of C–O–H fluids. *Lithos* **55**, 101–114.

Huizenga, J.M., Touret, J.L.R., 1999. Fluid inclusions in shear zones: the case of the Umwindshi shear zone in the Harare–Shamva–Bindura greenstone belt, NE Zimbabwe. *Eur. J. Mineral.* **11**, 1079–1090.

Johnson, E.L., Hollister, L.S., 1995. Syndeformational fluid trapping in quartz: determining the pressure–temperature conditions of deformation from fluid inclusions and the formation of pure CO_2 fluid inclusions during grain boundary migration. *J. Metamorphic Geol.* **13**, 239–249.

Johnson, J.W., Oelkers, E.H., Helgeson, H.C., 1992. SUPRCRT92: a software package for calculating the standard molal thermodynamic properties of minerals, gases, aqueous species, and reactions from 1 to 5000 bar and 0 to 1000 °C. *Comp. Geosci.* **18**, 899–947.

Kerrich, R., 1976. Some effects of tectonic recrystallization on fluid inclusions in vein quartz. *Contrib. Mineral. Petrol.* **59**, 195–202.

Lepland, A., Arrhenius, G., Cornell, D., 2002. Apatite in early Archean Isua supracrustal rocks, southern West Greenland: its origin, association with graphite and potential as a biomarker. *Precamb. Res.* **118**, 221–241.

Luque, F.J., Pasteris, J.D., Wopenka, B., Rodas, M., Barrenechea, J.F., 1998. Natural fluid-deposited graphite: mineralogical characteristics and mechanisms of formation. *Am. J. Sci.* **298**, 471–498.

Marshall, B., Giles, A.D., Hagemann, S.G., 2000. Fluid inclusions in metamorphic and synmetamorphic (including metamorphogenic) base and precious metal deposits: indicators of ore-forming conditions and/or ore-modifying histories? In: Spry, P.G., Marshall, B., Vokes, F.M. (Eds.), *Metamorphosed and Metamorphogenic Ore Deposits. Rev. Econ. Geol.* **11**, 119–148.

Mavrogenes, J.A., Bodnar, R.J., 1994. Hydrogen movement into and out of fluid inclusions in quartz: experimental evidence and geologic implications. *Geochim. Cosmochim. Acta* **58**, 141–148.

Mojzsis, S.J., Arrhenius, G., McKeegan, K.D., Harrison, T.M., Nutman, A.P., Friend, C.R.L., 1996. Evidence for life on Earth before 3,800 million years ago. *Nature* **384**, 55–59.

Moorbath, S., 2005. Dating earliest life. *Nature* **434**, 155.

Moorbath, S., O'Nions, R.K., Pankhurst, R.J., 1973. Early Archean age for the Isua iron formation, West Greenland. *Nature* **245**, 138–139.

Moorbath, S., Allaart, J.H., Bridgwater, D., McGregor, V.R., 1977. Rb–Sr ages on early Archaean supracrustal rocks and Amîtsoq gneisses at Isua. *Nature* **270**, 43–45.

Morgan, G.B., Chou, I.M., Pasteris, J.D., Olsen, S.N., 1993. Re-equilibration of CO_2 fluid inclusions at controlled hydrogen fugacities. *J. Metamorphic Geol.* **11**, 155–164.

Myers, J.S., 2002. Protoliths of the 3.8–3.7 Ga Isua greenstone belt, West Greenland. *Precamb. Res.* **105**, 129–141.

Nakamura, K., Katu, Y., 2004. Carbonatization of oceanic crust by the seafloor hydrothermal activity and its sigificance as a CO_2 sink in the Early Archean. *Geochim. Cosmochim. Acta* **68**, 4595–4618.

Naraoka, H., Ohtake, M., Maruyama, S., Ohmoto, H., 1996. Non-biogenic graphite in 3.8 Ga metamorphic rocks from the Isua district, Greenland. *Chem. Geol.* **133**, 251–260.

Nutman, A.P., McGregor, V.R., Friend, C.R.L., Bennett, V.C., Kinny, P.D., 1996. The Itsaq Gneiss Complex of southern West Greenland; the world's most extensive record of early crustal evolution (3900–3600 Ma). *Precamb. Res.* **78**, 1–39.

Nutman, A.P., Friend, C.R.L., Bennett, V.C., 2002. Evidence for 3650–3600 Ma assembly of the northern end of the Itsaq Gneiss Complex, Greenland: implication for early Archean tectonics. *Tectonics* **21**, 1–28.

Nutman, A.P., Friend, C.R.L., Bennett, V.C., McGregor, V.R., 2004. Dating the Ameralik dyke swarms of the Nuuk district, southern West Greenland: mafic intrusion events starting from c. 3510 Ma. *J. Geol. Soc. London* **161**, 421–430.

Ohmoto, H., Kerrick, D., 1977. Devolatization equilibria in graphitic systems. *Am. J. Sci.* **277**, 1013–1044.

Orione, P., Conte, R., Frezzotti, M.L., Ferrando, S., Compagnoni, R., 2003. Rodingitisation of a basaltic dyke induced by H_2O–$CaCl_2$–NaCl–H_2–CH_4 reduced fluids in the Bellecombe serpentinite, Piemonte zone, Aosta valley, Italian western Alps. ECROFI XVII. *Acta Mineral. Petrogr.*, Budapest. p. 151 (abstr.).

Passchier, C.W., Trouw, R.A.J., 1996. *Microtectonics*. Springer-Verlag, Berlin Heidelberg, pp. 289.

Pasteris, J.D., 1999. Causes of the uniformly high crystallinity of graphite in large epigenetic deposits. *J. Metamorphic Geol.* **17**, 779–787.

Pasteris, J.D., Chou, I.M., 1998. Fluid-deposited graphitic inclusions in quartz: comparison between KTB (German Continental Deep-Dril-

ling) core samples and artificially reequilibrated natural inclusions. *Geochim. Cosmochim. Acta* **62**, 109–122.

Peretti, A., Dubessy, J., Mullis, J., Frost, R.B., Trommsdorff, V., 1992. Highly reducing conditions during Alpine metamorphism of the Malenco peridotite (Sondrio, northern Italy) indicated by mineral paragenesis and H_2 in fluid inclusions. *Contrib. Mineral. Petrol.* **112**, 329–340.

Perry, E.C., Ahmad, S.N., 1977. Carbon isotope composition of graphite and carbonate minerals from 3.8 AE metamorphosed sediments, Isukasia, Greenland. *Earth Planet. Sci. Lett.* **36**, 280–284.

Pichavant, M., Ramboz, C., Weisbrod, A., 1982. Fluid immiscibility in natural processes: use and misuse of fluid inclusion data: I. Phase equilibria analysis—a theoretical and geometrical approach. *Chem. Geol.* **37**, 1–27.

Ramboz, C., Pichavant, M., Weisbrod, A., 1982. Fluid immiscibility in natural processes: use and misuse of fluid inclusion data: II. Interpretation of fluid inclusion data in terms of immiscibility. *Chem. Geol.* **37**, 29–48.

Ramboz, C., Schnapper, D., Dubessy, J., 1985. The P–V–T–X–f_{O_2} evolution of H_2O–CO_2–CH_4-bearing fluid in a wolframite vein: reconstruction from fluid inclusion studies. *Geochim. Cosmochim. Acta* **49**, 205–219.

Roedder, E., 1984. Fluid Inclusions. *Mineral. Ass. Am. Rev. Mineral.* **12**, 644.

Rollinson, H.R., 2002. The metamorphic history of the Isua Greenstone Belt, West Greenland. In: Fowler, C.M.R., Ebinger, C.J., Hawkesworth, C.J. (Eds.), *The Early Earth: Physical, Chemical and Biological Development*. *Geol. Soc. London Spec. Pub.* **199**, 329–350.

Rollinson, H.R., 2003. Metamorphic history suggested by garnet-growth chronologies in the Isua Greenstone Belt, West Greenland. *Precamb. Res.* **126**, 181–196.

Rose, N.M., Rosing, M.T., Bridgewater, D., 1996. The origin of metacarbonate rocks in the Archaean Isua supracrustal belt, West Greenland. *Am. J. Sci.* **296**, 1004–1044.

Rosing, M.T., 1999. ^{13}C-depleted carbon microparticles in >3700 Ma seafloor sedimentary rocks from West Greenland. *Science* **283**, 674–676.

Rosing, M.T., Rose, N.M., 1993. The role of ultramafic rocks in regulating the concentration of volatile and non-volatile components during deep crustal metamorphism. *Chem. Geol.* **108**, 187–200.

Rosing, M.T., Rose, N.M., Bridgewater, D., Thomson, H.S., 1996. Earliest part of Earth's stratigraphic record: a reappraisal of the >3.7 Ga Isua (Greenland) supracrustal sequence. *Geology* **24**, 43–46.

Ryzhenko, B.N., Volkov, V.P., 1971. Fugacity coefficients of some gases in a broad range of temperatures and pressures. *Geochem. Int.*, 468–481.

Schidlowski, M., 2001. Carbon isotopes as biogeochemical recorders of life over 3.8 Ga of Earth history: evolution of a concept. *Precamb. Res.* **106**, 117–134.

Schidlowski, M., Appel, P.W.U., Eichmann, R., Junge, C.E., 1979. Carbon isotope geochemistry of the 3.7×10^9 yr. old Isua sediments, West Greenland: implications for the Archean carbon and oxygen cycles. *Geochim. Cosmochim. Acta* **43**, 189–199.

Schmidt, C., Bodnar, R.J., 2000. Synthetic fluid inclusions: XVI. PVTX properties in the system H_2O–NaCl–CO_2 at elevated temperatures, pressures and salinities. *Geochim. Cosmochim. Acta* **64**, 3853–3869.

Shi, P., Saxena, S.K., 1992. Thermodynamic modeling of the C–H–O–S fluid system. *Am. Mineral.* **77**, 1038–1049.

Solvang, M., 1999. *An investigation of metavolcanic rocks from the eastern part of the Isua Greenstone Belt, Western Greenland*. Danmark Grønlands Geol. Unders. (GEUS) internal report, 62 pp.

Sterner, S.M., Hall, D.L., Bodnar, R.J., 1988. Synthetic fluid inclusions. V. Solubility relations in the system NaCl–KCl–H_2O under vapor-saturated conditions. *Geochim. Cosmochim. Acta* **52**, 989–1005.

Sterner, S.M., Hall, D.L., Keppler, H., 1995. Compositional re-equilibration of fluid inclusions in quartz. *Contrib. Mineral. Petrol.* **119**, 1–15.

Touret, 1981. Fluid inclusions in high-grade metamorphic rocks. In: Hollister, L.S., Crawford, M.L. (Eds.), *Short Course in Fluid Inclusions: Applications to Petrology*. Min. Ass. Canada, vol. 6, pp. 182–208.

Touret, J.L.R., 2001. Fluids in metamorphic rocks. *Lithos* **55**, 1–25.

Touret, J.L.R., 2003. Remnants of early Archaean hydrothermal methane and brines in pillow-breccia from the Isua Greenstone Belt, West Greenland. *Precamb. Res.* **126**, 219–233.

Ueno, Y., Yurimoto, H., Yoshioka, T., Maruyama, S., 2002. Ion microprobe analyses of graphite from ca. 3.8 Ga metasediments, Isua supracrustal belt, West Greenland: relationship between metamorphism and carbon isotopic composition. *Geochim. Cosmochim. Acta* **66**, 1257–1268.

Urai, J.L., Spiers, C.J., Zwart, H.J., Lister, G.S., 1986. Weakening of rock salt by water during long term creep. *Nature* **324**, 554–557.

van den Kerkhof, A.M., Kronz, A., Simon, K., Scherer, T., 2004. Fluid-controlled quartz recovery in granulite as revealed by cathodoluminescence and trace element analyses (Bamble sector, Norway). *Contrib. Mineral. Petrol.* **146**, 637–652.

Van Zuilen, M.A., Lepland, A., Arrhenius, G., 2002. Reassessing the evidence for the earliest traces of life. *Nature* **418**, 627–629.

Van Zuilen, M.A., Lepland, A., Teranes, J., Finarelli, J., Wahlen, M., Arrhenius, G., 2003. Graphite and carbonates in the 3.8 Ga old Isua Supracrustal Belt, southern West Greenland. *Precamb. Res.* **126**, 331–348.

Waters, J.C., Wallace, D.B., 1992. Volcanology and sedimentology of the host succession to the Hellyer and Que River volcanic-hosted massive sulfide deposits, northwestern Tasmania. *Econ. Geol.* **87**, 650–666.

Wilkins, R.W.T., Barkas, J.P., 1978. Fluid inclusions, deformation and recrystallization in granite tectonites. *Contrib. Mineral. Petrol.* **65**, 293–299.

Wilson, M., 1989. *Igneous petrogenesis, a global tectonic approach*. Unwin Hyman, London, pp. 466.

Zen, E., 1985. An oxygen buffer for some peraluminous granites and metamorphic rocks. *Am. Miner.* **70**, 65–73.